Vilnius University

Faculty of Physics

Neenu Kelamangalath Sajeevan

INVESTIGATION OF ELECTRICAL PROPERTIES OF STRONTIUM TITANATE, IN WHICH Sr IS PARTIALLY SUBSTITUTED BY La, Gd OR Nd

Master's final thesis

Electronics and Telecommunication Technologies study programme

Student	Neenu Kelamangalath Sajeevan
Approved	2026-05-22
Academic supervisor	Dr. Tomas Šalkus
Director of the Institute of Applied Electrodynamics and Telecommunications	Prof. Robertas Grigalaitis

Vilnius 2026

Contents

1. Introduction

Strontium titanate, $SrTiO_3$, is an important perovskite material used in electrical and dielectric studies. In this study, $SrTiO_3$ was selected as the base material to analyse how different dopants change its electrical behaviour. The pure $SrTiO_3$ has low conductivity at room temperature, but this can change when dopants are added.

In this study, $SrTiO_3$ samples doped with La, Gd and Nd were investigated. These dopants can change the charge balance inside the material. This can lead to the formation of defects such as oxygen vacancies. These defects can affect both the ionic movement and electronic response, when the temperature is increased.

The Impedance spectroscopy set up was used to study the electrical behaviour of the samples. This method gives the response of a material over a wide range of frequencies. It also helps to separate different contributions, such as grain, grain boundary and electrode effects. From the impedance spectra and equivalent circuit fitting, resistance values could be obtained. These values were later used for conductivity and activation energy calculations.

The samples used in this work include undoped $SrTiO_3$ and $SrTiO_3$ doped with La, Gd and Nd. YSZ was also used as a reference sample because it mainly shows ionic conduction. This made it possible to compare the doped $SrTiO_3$ samples with a material whose ionic behaviour is already well known.

The dielectric response was also analysed for one selected sample, $Sr_{0.7}Nd_{0.2}TiO_3$. In this part, dielectric permittivity, dielectric loss and relaxation time were studied from the available dielectric data.

The aim of this work is to compare how La, Gd and Nd doping changes the electrical behaviour of $SrTiO_3$-based ceramics. The study mainly focuses on impedance spectra, ionic and electronic conductivity, activation energy and dielectric relaxation of one of the selected Nd-doped sample.

2. Literature Overview

2.1. $SrTiO_3$ Structure and Substitution Possibilities

$SrTiO_3$ is a cubic perovskite oxide material as shown in figure 1. Its structure follows the ABO_3 form, where Sr is present in the A-site and Ti is present in the B-site. This type of structure allows different ions to enter the lattice and change the material properties. When substitution happens at the A-site or B-site, it can create lattice strain or defects such as oxygen vacancies. These changes can later affect the conductivity and dielectric behaviour of the material *[1].* In this work, the main focus is on A-site substitution, where Sr^{2+} is partly replaced by rare-earth dopants such as La^{3+}, Gd^{3+} and Nd^{3+}.

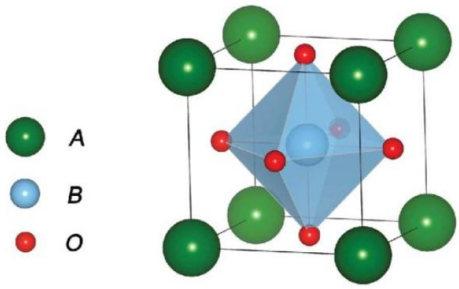

Fig. 1: The ideal structure of ABO_3 perovskite compounds *[2]*

Gadolinium Doping

Gd^{3+} doping can change the structure and electrical behaviour of $SrTiO_3$. In this doping a part of the Sr sites can be occupied by Gd atoms. This substitution slightly reduces the lattice size and makes Sr vacancies more stable. For example, when 12.5% Gd is added, the lattice constant decreases from about 3.94 Å to nearly 3.92 Å. *[3]*.

Adding Gd is also energetically more favourable than creating separate Sr or oxygen vacancies, mainly under oxygen-rich conditions. The bandgap shows a small increase from around 1.9 eV to 1.96 eV, which suggests a small change in the electronic structure *[3]*.

Lanthanum Doping

Lanthanum (La^{3+}) is one of the common donor dopants that is used on the A-site of the $SrTiO_3$ perovskite structure to introduce n-type electronic charge carriers. Substitution of Sr^{2+} with La^{3+} creates extra electrons in the system to maintain charge neutrality. Therefore, La-doped $SrTiO_3$ has been widely investigated for its electrical transport behavior, especially at higher temperatures where charge transport becomes more active *[4]*.

Additionally, studies report that moderate La substitution significantly increases electronic conduction in $SrTiO_3$, and in some cases can transform it from an insulating to a highly conductive or semimetal-like material compared to undoped $SrTiO_3$. In reducing atmospheres and under high temperature, lanthanum dopants facilitate the formation of Ti^{3+} from Ti^{4+}, which increases free electron concentration and enhances electrical conduction *[5]*.

In addition to enhanced electronic transport, defects and non-stoichiometry associated with La doping may also introduce oxygen vacancies and defect complexes that contribute to mixed ionic–electronic conduction under certain conditions. For example, A-site deficiency or co-doping strategies have been shown to increase partial ionic conductivity in La-based systems *[6]*.

La-doped $SrTiO_3$ systems have drawn interest not only for fundamental transport studies, but also for application in thermoelectric materials, solid oxide fuel cell electrodes, and other oxide electronic devices where high n-type conductivity and thermal stability are desirable *[7]*.

Neodymium Doping

Neodymium (Nd^{3+}) is one of the rare-earth dopant which can replace Sr^{2+} at the A-site of $SrTiO_3$. Since Nd^{3+} has a different charge and ionic size compared to Sr^{2+}, some local lattice

changes may appear after doping. However, the overall cubic structure of $SrTiO_3$ is generally retained *[8]*.

After Nd is introduced into the $SrTiO_3$ lattice, the material tries to maintain charge balance. This may happen through oxygen vacancy formation or by partial conversion of Ti^{4+} to Ti^{3+}. Such defects can later influence the electrical response of the material, especially at elevated temperatures *[8]*.

Some studies also reported that Nd substitution can affect dielectric response and lattice-related behaviour in $SrTiO_3$. Temperature-dependent dielectric changes were observed, showing that Nd doping interacts with the crystal lattice and polarization behaviour of the material *[9]*.

Neodymium addition may also influence the microstructure after sintering, including grain size and density changes depending on the doping amount. Even though the main crystal structure is mostly retained, Nd doping still introduces some defect-related and structural changes in $SrTiO_3$ *[8]*.

Overall, Nd doping changes the electrical and dielectric behaviour of $SrTiO_3$ while the main perovskite structure remains largely unchanged.

2.2.Electrical Properties of Doped $SrTiO_3$

The electrical response of $SrTiO_3$ changes after doping. Pure $SrTiO_3$ normally has low conductivity at room temperature. When dopants are added, extra charge carriers or oxygen vacancies can be created in the material. Because of this, the conductivity can change with dopant type, dopant amount and temperature.

Conductivity Mechanisms in Doped STO

In doped $SrTiO_3$, the charge transport is mainly linked with donor substitution and defects. When La^{3+}, Gd^{3+} or Nd^{3+} goes into the Sr^{2+} position, the charge balance of the lattice changes. The material can balance this by producing free electrons or by forming defects such as oxygen vacancies. These oxygen vacancies can also help in the formation of Ti^{3+} states, which affects the electronic conduction *[8][11]*.

Gadolinium (Gd) Doping

Gd substitution at the Sr-site can affect charge compensation and defect formation in $SrTiO_3$. Since Gd^{3+} replaces Sr^{2+}, the charge difference may be balanced by defects such as oxygen vacancies or other defect centres. These defects can influence both ionic and electronic conductivity, mainly at higher temperatures where charge movement becomes easier.

Gd doping may also change the electronic structure of $SrTiO_3$. Localized electronic states can appear near the conduction band, and this may support electronic conduction. Also, since Gd^{3+} is smaller than Sr^{2+}, a small lattice contraction may happen. Even with this change, the main perovskite structure is usually maintained, so Gd can modify the electrical behaviour without fully changing the $SrTiO_3$ lattice *[3] [10]*.

Lanthanum (La) Doping

Lanthanum is also used as a donor dopant in $SrTiO_3$. When La^{3+} replaces Sr^{2+}, extra electrons can be introduced to balance the charge difference. Because of this, La-doped $SrTiO_3$ usually shows better conductivity than pure $SrTiO_3$, especially when the temperature is increased *[12].*

La addition can also affect the defect behaviour of $SrTiO_3$. At higher temperature, oxygen vacancies and other defect-related changes may take part in the conduction process. These effects can influence both the bulk and grain boundary regions of the sample, which is why La-doped $SrTiO_3$ gives a clear temperature-dependent response in impedance measurements *[7] [13].*

La-doped $SrTiO_3$ has also been studied for thermoelectric materials, solid oxide fuel cell electrodes and other high-temperature ceramic applications. This is mainly because it can show good conductivity and stability at elevated temperature *[12] [13].*

Neodymium (Nd) Doping

Neodymium doping can also modify the conductivity behaviour of $SrTiO_3$. After Nd^{3+} enters the Sr-site, the charge balance inside the material is disturbed slightly. To compensate this, extra electrons or oxygen vacancies may appear in the lattice. These changes can later contribute to charge transport, especially at higher temperatures *[8].*

In Nd-doped $SrTiO_3$, partial conversion of Ti^{4+} to Ti^{3+} may also occur during charge compensation. Because of this, both defect formation and electronic changes can influence the overall conductivity behaviour of the material *[8].*

The conductivity response is also influenced by factors such as doping amount, grain boundaries and the microstructure formed after sintering. Therefore, Nd-doped $SrTiO_3$ is often used when studying how rare-earth substitution affects ionic and electronic transport in $SrTiO_3$ ceramics.

2.3.Ionic Conduction in Zirconia-Based Ceramics (YSZ)

Zirconia-based ceramics stabilized with trivalent dopants such as yttrium is included in this work because it is widely known as an oxygen ion conductor. In zirconia, yttrium doping helps to create oxygen vacancies. These vacancies give oxygen ions a path to move through the structure. Because of this, YSZ shows good ionic conductivity, while the electronic contribution is very small in normal conditions. This is also the reason why YSZ is widely used as an electrolyte material in solid oxide fuel cells and other electrochemical devices *[14].*

Impedance spectroscopy studies on stabilized zirconia show that the electrical response can be separated into bulk, grain boundary and electrode contributions. In Nyquist plots, these contributions usually appear as semicircular arcs, especially at higher temperatures. This clear ionic response makes zirconia-based ceramics useful as reference materials when studying purely ionic conduction behaviour *[14].*

The bulk conductivity of stabilized zirconia is mostly independent of oxygen partial pressure, which shows that the charge transport is mainly ionic. Under normal measurement conditions, the electronic contribution is very small. Because the ionic conduction mechanism of YSZ is already well understood, it was used in this research as a reference material. This helped to

compare pure ionic conduction with the mixed ionic–electronic conduction observed in $SrTiO_3$ and doped $SrTiO_3$ ceramics *[14] [15].*

2.4. Dielectric Relaxation in $SrTiO_3$-Based Ceramics

Dielectric relaxation shows how the material responds when the applied frequency and temperature are changed. In dielectric measurements, ε′ is used to describe the permittivity part, while ε″ is related to dielectric loss. By looking at these two values, it is possible to understand how polarization and loss processes change with frequency *[16].*

In $SrTiO_3$-based ceramics, the relaxation behaviour can be affected by defects, oxygen vacancies, local polar regions and charge movement. Because more than one contribution can be present, the dielectric response may not always follow one simple relaxation process. In non-stoichiometric $SrTiO_3$ ceramics, different relaxation behaviours have been connected with polar nanoregions, charged defects and hopping-type charge transport. *[17].*

Rare-earth substitution can also influence the dielectric behaviour of $SrTiO_3$ ceramics. In Sm-substituted $SrTiO_3$, two dielectric loss peaks were seen, and the authors related this relaxation behaviour to oxygen vacancies. This gives a useful background for understanding how defect formation can affect dielectric relaxation in rare-earth doped $SrTiO_3$ ceramics *[18].*

In some doped $SrTiO_3$ systems, the relaxation behaviour may also deviate from a simple Arrhenius trend. For example, Nb-doped $SrTiO_3$ single crystals showed an anomalous dielectric relaxation peak, where the peak position changed differently from normal thermally activated relaxation. This behaviour was related to polar nanoregions, carrier concentration and interface-related effects *[19].*

3. Experimental Setup

3.1. Sample Preparation

The samples used in this work include pure $SrTiO_3$ together with several A-site doped $SrTiO_3$ compositions containing Gd, La and Nd. The samples were $SrTiO_3$, $Sr_{0.85}Gd_{0.1}TiO_3$, $Sr_{0.7}Gd_{0.2}TiO_3$, $Sr_{0.85}La_{0.1}TiO_3$, $Sr_{0.7}La_{0.2}TiO_3$, $Sr_{0.75}La_{0.25}TiO_3$, $Sr_{0.55}La_{0.3}TiO_3$, $Sr_{0.65}La_{0.35}TiO_3$, $Sr_{0.85}Nd_{0.1}TiO_3$ and $Sr_{0.7}Nd_{0.2}TiO_3$. All these ceramics were sintered at Le Mans University, France. YSZ was also included as a reference sample because it mainly shows ionic conduction. This made it easier to compare its impedance response with the mixed ionic–electronic behaviour observed in the $SrTiO_3$-based samples.

Additionally, different doping concentrations were chosen to understand how the amount of dopant affects the electrical behaviour of $SrTiO_3$. By changing the composition, the level of substitution at the A-site also changes, which can affect the charge carriers and defect formation in the material. The samples were analysed using impedance spectroscopy, and the results were compared with the undoped $SrTiO_3$ sample to see how doping influences the overall electrical properties.

Before the impedance analysis, the measurements of these samples (length and diameter) were taken to calculate the electrode area. This value was needed as an input parameter during the impedance spectroscopy setup. After the measurement, the samples were coated with thin layer of platinum on their surface to serve as electrodes. This coating ensures stable and good electrical contact during impedance spectroscopy measurements. These coated samples are then subjected to two-step heating process in the oven. Initially, the sample was heated at 400°C for 1 hour and then at 800°C for another 20 minutes. This heat treatment is done to stabilize the electrode contacts. Once the samples were cooled to the room temperature these samples were placed in the impedance spectrometer for electrical measurement.

3.2. Impedance Spectroscopy

Impedance spectroscopy is a commonly used method to study the electrical behaviour of materials over a wide range of frequencies. It is commonly used for the measurement of electronic conductivities of electroceramic materials like $SrTiO_3$ that exhibit both ionic and electronic properties. Impedance spectroscopy applies a small AC signal and then shows how the current behaves at different frequencies. The impedance is expressed as a complex value:

$$Z(\omega)=Z'+jZ'' \qquad (1)$$

where Z' is the real part (resistive) and Z'', is the imaginary (reactive) part.

By analysing the frequency response at different temperatures, several data such as grain and grain boundary conduction, polarization effects, and electrode reactions, can be studied/analysed separately. Additionaly, impedance spectroscopy is highly sensitive even to small variations, and this will help us to understand how the structure, defects, or dopants affect the electrical properties of our ceramic samples *[20] [21].*

Working Principle

The basic idea of impedance spectroscopy is to see how the sample responds when a small AC signal is applied. In a DC measurement, only one resistance value is usually obtained. But in impedance spectroscopy, the response is measured at different frequencies. Because of this, it gives more information about the sample, such as whether the resistance is mainly coming from grains, grain boundaries or electrode effects. It also helps to study ionic and electronic contributions separately *[20].*

In ceramic materials, the current generated by the applied AC signal is usually very small (nanoampere or microampere) range. Measuring this tiny current directly will not give us accurate results. So, an I–V (current-to-voltage) converter is used in the system. This converter is usually a transimpedance amplifier, which is a type of operational amplifier circuit. It uses a precision feedback resistor R_f to convert the current into a measurable voltage:

$$V_{out}=-I\times R_f \qquad (2)$$

This output voltage V_{out} represents the current, and it is easier to measure accurately. The sign is negative due to the op-amp configuration, but in impedance spectroscopy only magnitude and phase is considered *[22]*.

After the current is converted to voltage using the I–V converter, it is sent to Channel 1 (CH1) of the digital oscilloscope or impedance analyser. Meanwhile, the original applied voltage signal is recorded by Channel 2 (CH2). The CH1 measures the output of the I–V converter (i.e., the current signal, converted into voltage) and the CH2 measures the reference AC voltage that was applied to the sample.

These two signals allow the system to calculate both the magnitude and phase angle of impedance at each frequency. The phase difference between CH1 and CH2 is really important, as it helps separate resistive vs. capacitive behaviour. This dual-channel oscilloscope approach is standard in high-resolution impedance setups *[23]*.

Experimental Setup

In our experiment set up, the sample was kept between two platinum electrodes inside a temperature-controlled furnace chamber. The main parts of the measurement setup were:

- A function generator (internal to the IS system),
- The ceramic sample connected to measurement leads,
- An I–V converter to transform current to voltage,
- A dual-channel Handyscope HS3 model oscilloscope or analyser to capture voltage across the sample and current through it.

The block diagram showing the impedance spectrometer set-up is shown in Figure 2. Since the measured current across the sample was very small, it could not be read directly with good accuracy. For this reason, an op-amp-based current-to-voltage converter was used. A precision feedback resistor, Rf, helped convert the sample current into a measurable voltage signal. This output signal was then recorded through Channel 1(CH1), while the applied voltage was recorded through Channel 2(CH2).

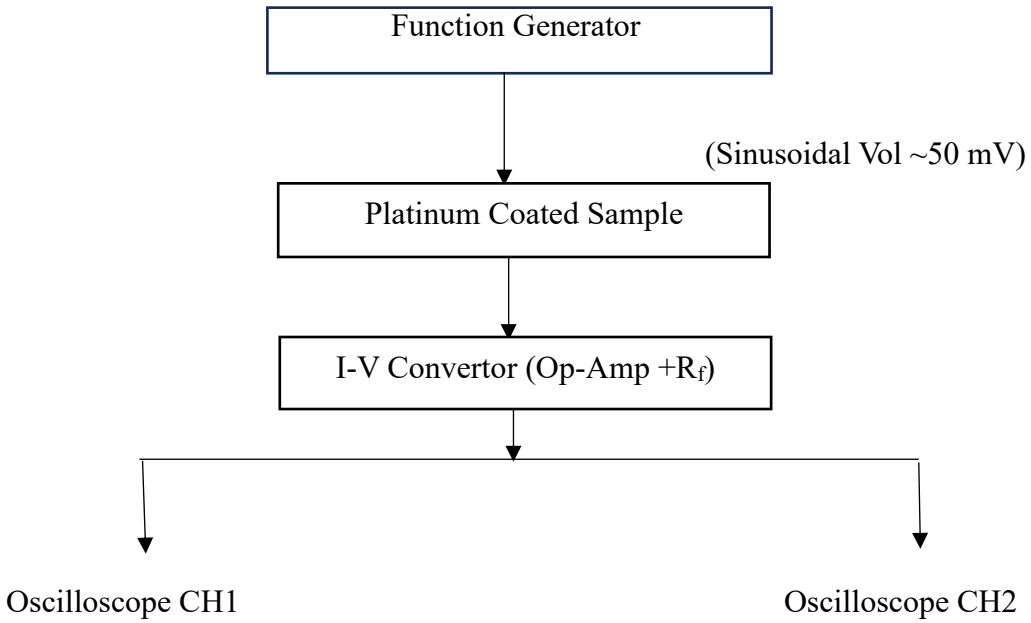

(I signal as Vout) (Applied Voltage)

Data saved as `.mat` → converted to `.DAT` for ZView

Fig. 2: Block diagram of impedance spectrometer set-up

The samples were placed in the impedance spectroscopy for electrical measurement. The measurements were carried out for wide range of temperatures from 300 K to 800 K. The complete measurement process for each sample took approximately 4-5 hours, ensuring sufficient time at each temperature for accurate data capture.

The heating was controlled using a computer-operated DC power. A thermocouple probe connected to an Amprobe TMD90A digital thermometer was used to monitor the sample temperature by direct contact with the side of the ceramic pellet. This thermometer also acted as the feedback sensor for temperature regulation, enabling automatic temperature ramping.

The temperature was varied from room temperature up to 800 K. During measurements, the system increased temperature in range of 20 K. A small sinusoidal excitation voltage of 50 mV was applied to the sample to keep the response within the linear range and avoid self-heating effects. This setup allowed precise control over the experimental conditions and helped ensure accurate impedance data at each temperature point *[22].*

The impedance data collected was extracted using MATLAB. After this, the detailed analysis of the ionic and electronic behaviour of the materials as a function of temperature was performed.

3.3. Impedance Data Analysis

Once the measurements are completed for a temperature range of 300 K To 800 K, the final measurements are obtained in .mat file. This .mat file is exported and data is extracted using custom MATLAB script, which generated a .DAT file readable by the simulation software Z view. ZView, a specialized software tool used for impedance data fitting, equivalent circuit modelling, and extraction of physical parameters like resistance and capacitance values from complex impedance spectra *[20].*

Zview helps to analyse the experimental impedance data by fitting it with equivalent electrical circuits, that are constructed using basic electrical components like resistors (R), capacitors (C), and sometimes constant phase elements (CPE). In real ceramic materials like $SrTiO_3$, the impedance response is not always ideal, especially when grain boundaries, defects, or surface roughness are involved. That's why instead of using a pure capacitor in the equivalent circuit, a Constant Phase Element (CPE) is used. This element helps us model non-ideal capacitive behavior more accurately. The impedance of a CPE is described by the formula:

$$Z_{CPE} = \frac{1}{Q \cdot (j\omega)^P} \qquad (3)$$

Where Q is a constant (also called the CPE-T value) and has units similar to capacitance, it gives an idea of how strong the capacitive behaviour is.

P is the exponent, and it tells us how close the behaviour is to a perfect capacitor. If P = 1, the CPE behaves just like a pure capacitor. If P = 0, it acts like a pure resistor. In most real systems, P falls somewhere between 0.5 and 1, indicating some combination of resistive and capacitive behaviour *[24]*.

In short, these components of circuits help to model the physical processes occurring within the material, such as grain (bulk) conduction, and electrode interface behaviour.

Using ZView's fitting and simulation option, the simulation of these components were carried out to match the shape of the Nyquist curves and extracted values like R_1 and R_2 which were later analysed against temperature to find the conductivity and activation energies *[23]*.

While extracting the measured data in Zview, Nyquists plots received looks similar to the Fig. 3, and equivalent circuits were created as shown in the figure to each plot and the value of R_1 and R_2 were measured.

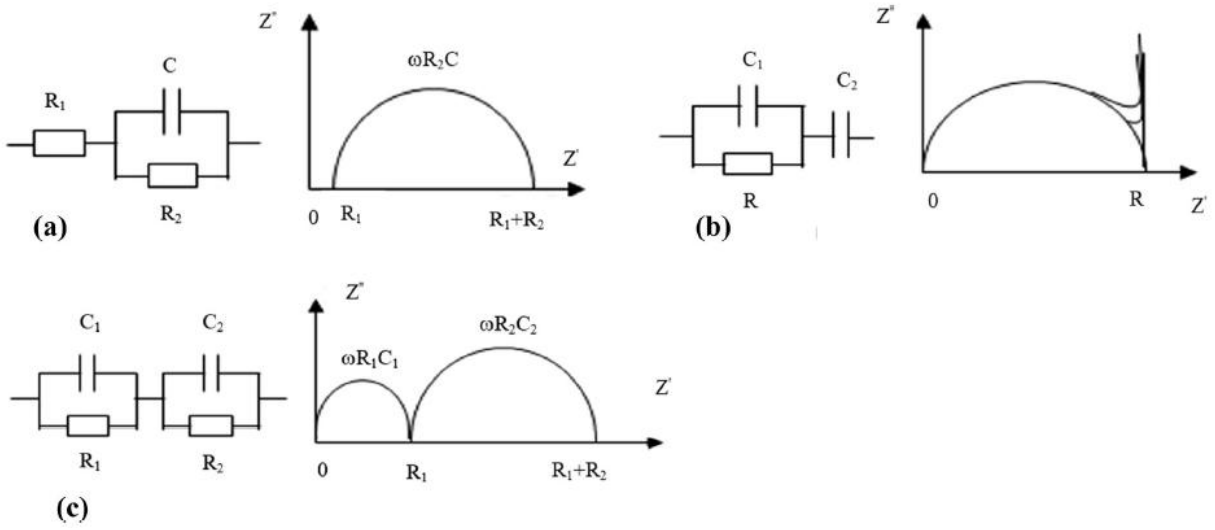

Fig. 3: Complex impedance plots for simple circuits RC of different combinations *[25]*

To explain further, this figure 3 shows the relationship between common equivalent circuits and their corresponding Nyquist plots, providing information on how to interpret the impedance data in electro ceramic materials like La-doped $SrTiO_3$. In subfigure 3(a), a parallel R–C element (representing grain or bulk behavior) is connected in series with another resistor (R_2), which could model grain boundary resistance. The corresponding Nyquist plot shows a single semicircle whose diameter reflects the sum of R_1 and R_2, but with the high-frequency arc dominated by $\omega R_1 C$.

Similarly, in subfigure (b), a more complex circuit is shown with two capacitive branches (C_1 and C_2) in series with a shared resistor. The resulting Nyquist plot exhibits a depressed semicircle, characteristic of systems with non-ideal capacitance or distributed relaxation times, which often occurs in ceramics with inhomogeneous microstructure or surface states.

Lastly, subfigure (c) displays two separate R–C elements, each generating its own semicircle in the Nyquist plot. The first arc corresponds to grain interior conduction, and the second to grain boundary impedance, with $\omega R_1 C_1$ and $\omega R_2 C_2$ controlling their respective frequency

responses. The horizontal projections (R_1 and R_2) allow the estimation of resistance values, which were later used in our study to calculate the slopes and activation energies. This figure provided a key reference for assigning physical meaning to the arcs seen in our measured spectra and for choosing appropriate fitting models in ZView.

However, in many ceramic materials, the Nyquist arcs are not perfectly semicircular. In some cases, the arc becomes slightly flattened or distorted instead of forming an ideal shape. This usually happens because the material itself is not fully uniform. Factors such as grain size variation, porosity and dopant distribution inside the ceramic can influence the impedance response. Because of this non-ideal behaviour, a constant phase element (CPE) was sometimes used in the equivalent circuit instead of a normal capacitor *[21]*.

The frequency is not shown directly on the Nyquist plot, but every point on the curve still belongs to one frequency value. In general, the high-frequency points appear on the left side of the arc. As the frequency becomes lower, the points move towards the right side. This is useful because faster responses, such as bulk conduction, are usually seen at higher frequencies, while slower grain boundary or electrode-related effects appear at lower frequencies *[25]*.

In this study of doped $SrTiO_3$ ceramics, the changes in the Nyquist plot, particularly the diameters and positions of the arcs were carefully tracked across different temperatures and doping levels. This helped us observe how the electrical resistivity evolved and how different dopants influenced ionic vs. electronic transport pathways. Using the extracted resistance values the graph conductivity versus 1000/T was plotted. This format reflects an Arrhenius-type thermally activated behavior, which is typical for ionic and electronic transport processes in doped ceramic materials.

After the conductivity graphs were plotted against 1000/T, the linear region was selected for each sample and fitted separately. The slope obtained from this region was then used to calculate the activation energy using the relation Ea = slope × 0.2. By comparing these activation energy values, it was possible to see how different dopants changed the conductivity behaviour and charge transport in the $SrTiO_3$-based ceramics.

3.4 Dielectric Data Analysis

In addition to the impedance spectroscopy data, dielectric data were also analysed for one selected sample, $Sr_{0.7}Nd_{0.2}TiO_3$. This dielectric measurement was not carried out directly instead the data was taken from previously recorded laboratory measurements. These data were used for plotting, fitting and relaxation time analysis.

These dielectric data were obtained using transmission coaxial dielectric spectroscopy. In this method, the sample is placed in a coaxial transmission-line type measurement system, and the dielectric/electrical response is analysed over a wide frequency range. The response is expressed using complex permittivity, where the real part ε' represents the dielectric permittivity and the imaginary part ε'' represents the dielectric loss. This type of measurement is useful for studying polarization response, dielectric loss and frequency-dependent relaxation behaviour in ceramic materials *[16]*.

For the analysis, the available ε′ and ε″ values were first plotted as a function of frequency at different temperatures. After this, the dielectric spectra were fitted using Origin software. Both ε′ and ε″ were fitted together, so that the same fitting model described the real and imaginary parts of the dielectric response. This was useful because the relaxation process affects both parts of the complex permittivity.

The fitting equation used in Origin was based on a multi-relaxation Havriliak-Negami type model. In Origin, the relaxation parts were written as HN_1, HN_2, and HN_3, together with a conductivity-related term. This type of model is useful when the dielectric response is broad and when more than one relaxation contribution may be present. Similar relaxation-type complex permittivity models are used in dielectric studies to describe non-ideal relaxation behaviour *[26]*.

The fitting model can be written in a simplified form as:

$$\varepsilon^*(\omega) = \varepsilon_\infty + HN_1 + HN_2 + HN_3 + \frac{\sigma}{(i\omega\varepsilon_0)^{n_s}} \qquad (4)$$

where,

$$HN_1 = \frac{\Delta\varepsilon_1}{[1 + (i\omega\tau_1)^{n_1}]^{h_1}}$$
$$HN_2 = \frac{\Delta\varepsilon_2}{[1 + (i\omega\tau_2)^{n_2}]^{h_2}}$$
$$HN_3 = \frac{\Delta\varepsilon_3}{[1 + (i\omega\tau_3)^{n_3}]^{h_3}}$$

and

$$\omega = 2\pi f$$

Here, $\varepsilon^*(\omega)$is the complex permittivity, $\varepsilon_\infty$is the high-frequency permittivity, and $\Delta\varepsilon_1$, $\Delta\varepsilon_2$, and $\Delta\varepsilon_3$are the dielectric strengths of the relaxation processes. The values τ_1, τ_2, and $\tau_3$are the relaxation times. The parameters n_1, n_2, n_3, h_1, h_2, and $h_3$describe the broadening and shape of each relaxation response. The last term represents the conductivity contribution, where $\sigma$is the conductivity-related parameter, $\varepsilon_0$is the vacuum permittivity, and $n_s$is the exponent used for the conductivity part.

In Origin, the real part of the calculated complex permittivity was fitted to the experimental ε′ data, while the imaginary part was fitted to the experimental ε″ data. From the fitted parameters, the relaxation time values were obtained. Although the model contains three possible relaxation terms, only two relaxation times were clearly used for further analysis in this work. These were marked as τ_1 and τ_2.

The extracted τ_1 and τ_2 values were later plotted against 1000/T to study how the relaxation behaviour changes with temperature. The detailed discussion of the dielectric spectra,

relaxation time trends and activation energy values is given in the Results and Discussion section.

4. Results and Discussions

4.1 Impedance Spectra of pure Ionic Conductor (YSZ)

As mentioned, YSZ was investigated as a reference pure ionic conductor to distinguish ionic conduction behaviour from the mixed ionic–electronic conduction observed in $SrTiO_3$ and doped $SrTiO_3$ ceramics. The impedance spectroscopy measurements were carried out at different temperatures to examine the characteristic impedance response of a purely ionic conductor.

Figure 4(a) shows the Nyquist plot of YSZ measured at 550 K. The impedance spectrum shows a partially developed semicircular arc followed by a pronounced low-frequency tail. The semicircular response is attributed to bulk and grain boundary ionic conduction, while the low-frequency tail is associated with electrode polarization effects, which are typical for pure ionic conductors *[14][15].*

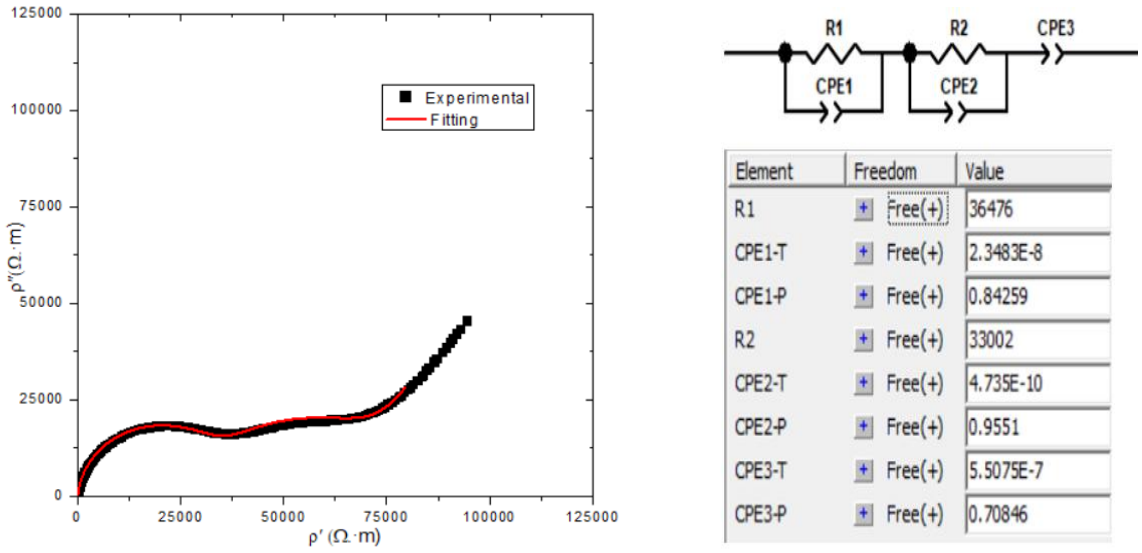

(a) (b)

Fig. 4(a): Experimental points, and fitting result for YSZ at 550K; (b): Equivalent circuit for YSZ at 550K.

When the higher temperature is considered, figure 5(a) shows the Nyquist plot of YSZ measured at 650 K.

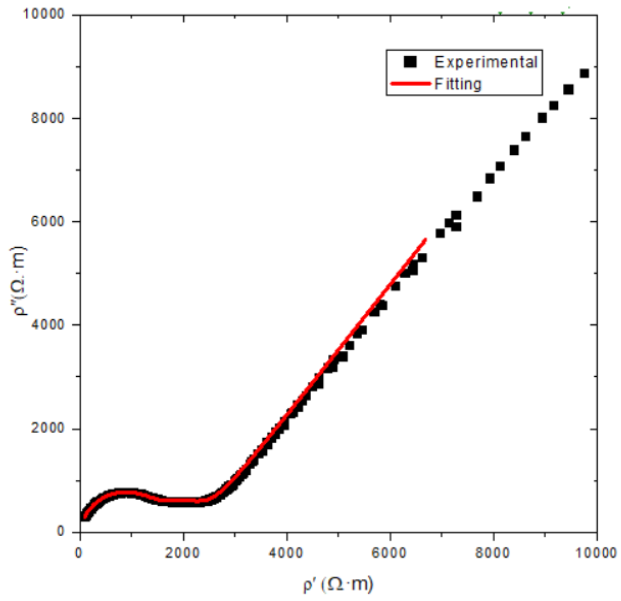

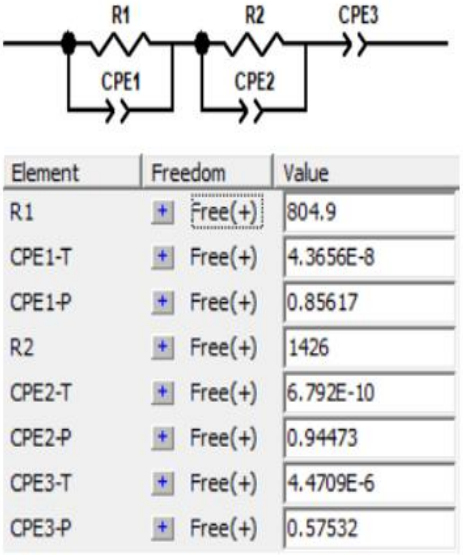

Element	Freedom	Value
R1	Free(+)	804.9
CPE1-T	Free(+)	4.3656E-8
CPE1-P	Free(+)	0.85617
R2	Free(+)	1426
CPE2-T	Free(+)	6.792E-10
CPE2-P	Free(+)	0.94473
CPE3-T	Free(+)	4.4709E-6
CPE3-P	Free(+)	0.57532

(a) (b)

Fig. 5(a): Experimental points, and fitting result for YSZ at 650K; (b): Equivalent circuit for YSZ at 650K.

When compared to 550 K, the size of the semicircular arc decreases highly, indicating a reduction in the overall ionic resistance with increasing temperature. The impedance response is dominated by a smaller arc followed by a steep low-frequency tail, suggesting enhanced bulk ionic conduction and persistent electrode polarization effects.

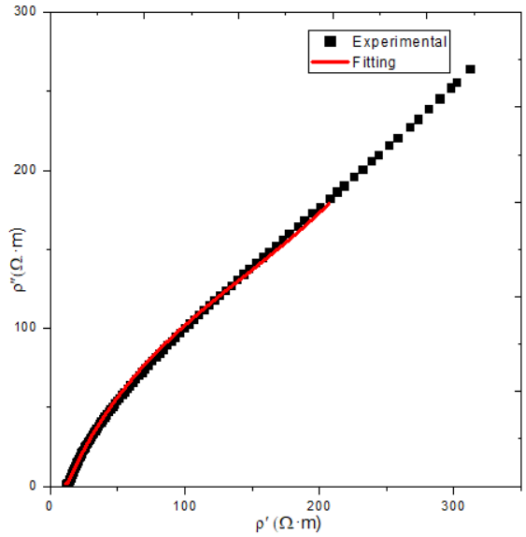

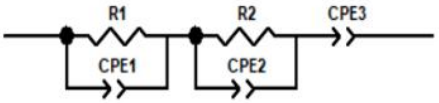

Element	Freedom	Value
R1	Free(+)	12.11
CPE1-T	Free(+)	1.2074E-7
CPE1-P	Free(+)	0.74391
R2	Free(+)	190.9
CPE2-T	Free(+)	4.0213E-5
CPE2-P	Free(+)	0.72303
CPE3-T	Free(+)	0.00011312
CPE3-P	Free(+)	0.694

(a) (b)

Fig. 6(a): Experimental points, and fitting result for YSZ at 750 K; (b): Equivalent circuit for YSZ at 750K.

Figure 6(a) shows the Nyquist plot of YSZ measured at 750 K. When compared to lower temperatures, the impedance spectrum exhibits a much smaller arc, indicating a significant

reduction in the overall ionic resistance with increasing temperature. The impedance response is dominated by a highly compressed arc followed by a steep low-frequency tail, which suggests enhanced bulk ionic conduction along with persistent electrode polarization effects *[14] [15]*.

Overall, the impedance spectra of YSZ show a clear and systematic reduction in resistive values with increasing temperature, which is characteristic of thermally activated ionic conduction. The Nyquist plots at all measured temperatures are dominated by well-defined ionic responses, both grain and grain boundary resistances with electrode polarization at low frequencies, confirming the negligible role of electronic conduction in this material. The consistent fitting using the same equivalent circuit across all temperatures further supports the stability of the ionic conduction mechanism in YSZ. This behaviour establishes YSZ as a suitable reference pure ionic conductor and provides a clear baseline for comparison with the mixed ionic–electronic conduction observed in $SrTiO_3$ and doped $SrTiO_3$ ceramics discussed in the following section.

4.2 Impedance spectra $SrTiO_3$ and doped $SrTiO_3$ ceramics

4.2.1 Impedance behaviour of undoped $SrTiO_3$

In this section, changes to the impedance spectra of undoped $SrTiO_3$ sample materials with the temperature is analysed. As discussed previously, the impedance data measured at different temperatures of 300 K to 800 K in impedance spectroscopy were analysed in the Zview and plotted using Origin software. The Nyquist plots for each sample were analysed after which fitting was performed by creating an equivalent circuit in Zview to determine the resistance contributions (R_1, R_2) associated with different processes in the material.

The significance of the equivalent circuit and its components such as resistance, capacitance and Constant Phase Elements (CPE) and their values are also discussed.

To begin with, the impedance data of $SrTiO_3$ sample measured at 540 K is considered.

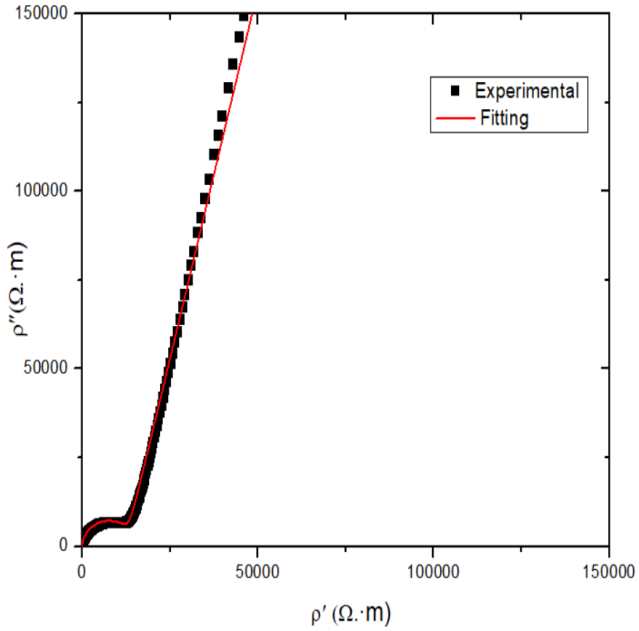

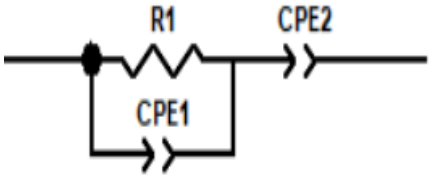

Element	Freedom	Value
R1	Free(+)	12302
CPE1-T	Free(+)	1.008E-9
CPE1-P	Free(+)	0.98948
CPE2-T	Free(+)	5.4934E-8
CPE2-P	Free(+)	0.84973

(a) (b)

Fig. 7(a): Experimental points, and fitting result for undoped $SrTiO_3$ at 540 K; (b): Equivalent circuit for $SrTiO_3$ at 540 K.

The figure 7(a) shows a Nyquist curve of $SrTiO_3$ at 540 K with a steep tail and no complete semicircle. The experimental results are plotted as squares, while the fitting is shown as a line. As seen in the graph, the fitting matches almost with the experimental data, which means that the equivalent circuit that used fits with the behaviour of the sample.

The equivalent circuit that used for fitting includes a resistor (R_1) and a constant phase element (CPE1) in parallel, and this combination is connected in series with another CPE (CPE2). This setup gave the best fitting result, because the response does not give a clean semicircle, and the long tail suggests some strong boundary effect. While the parallel part (R_1‖CPE1) appears to represent the grain interior, the CPE2 part represents non-ideal interfacial effects, where the grain boundary contribution is not clearly separated but may be included within this response.*[27]*.

The reason for choosing this circuit is that the shape of the Nyquist plot does not show the ideal/typical clearly-separated semicircles that are often linked to distinct grain and grain boundary responses. Instead of that it shows a steeply rising arc and a strongly sloped tail, which suggests a mix of overlapping processes.

The combination R_1‖CPE1 shows the response from bulk grains. As CPE1's power factor (P) is approximately near 1, it acts like a capacitor, with some non-ideal characteristics, that is only expected in real ceramics where perfect capacitive behaviour is rare. The R_1 connected in parallel captures the primary conductive behaviour of the grains *[28]*.

Explanation of elements

- R_1 = 12,302 Ω: This value shows the major resistive contribution of the sample. Normally, this value would reduce as temperature increases.
- CPE1 ($T = 1.008\times10^{-9}$, P = 0.98948): This component behaves like a capacitor but not exactly ideal. The power value (P) is approximately near to 1, therefore it's close to ideal. Hence it is probably representing the bulk or grain interior response.
- CPE2 ($T = 5.493\times10^{-8}$, P = 0.84973): These values also show a little more non-ideality. The P value is lower, so this one will be from grain boundaries or the electrode contact.

As shown in figure 7(a), at 540 K, the undoped $SrTiO_3$ sample showed a quite large impedance response. The plot has a steep arc rising above 150 000 Ω, which already tells us it's quite resistive. The R_1 value was calculated to be 12,302 Ω after fitting, which means the resistance is pretty high here. Also, the circuit fit followed the spectrum quite well. The high resistance might be due to the grain boundary related contribution. That being said, the CPE values are close to 1, showing it's behaving almost like ideal capacitors. That may suggest reasonably good electrochemical interface, but still, the charge transport wasn't that efficient.

Figure 8 (a) and (b) shows the experimental points and fitting result for undoped $SrTiO_3$ at 800 K and its equivalent circuit.

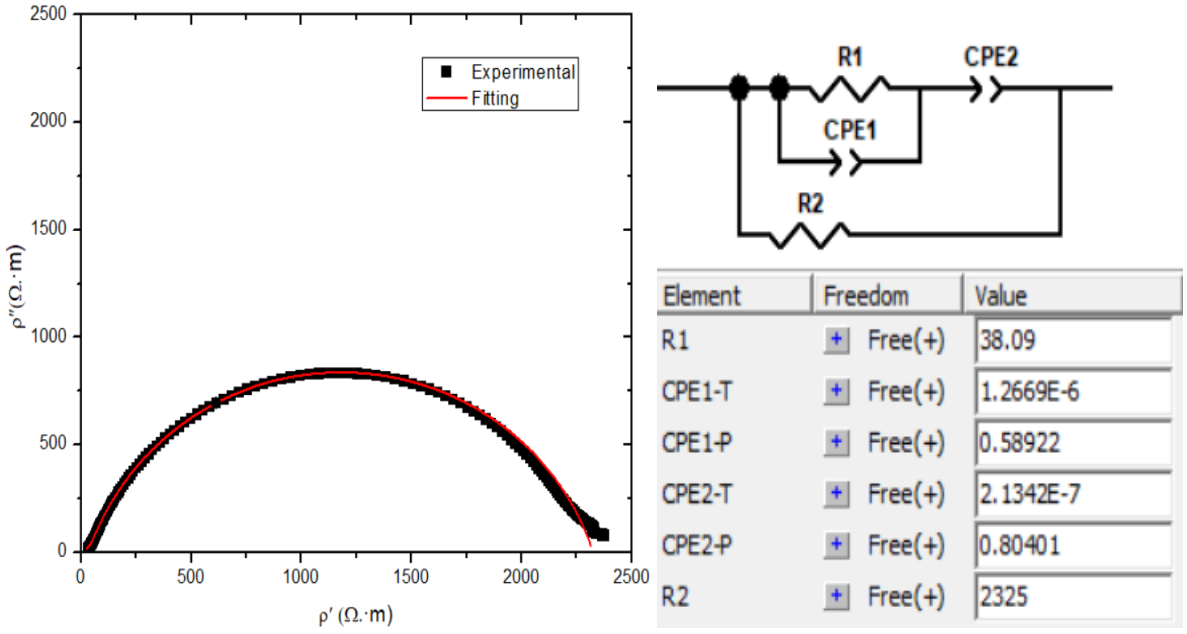

(a) (b)

Fig. 8.(a): Experimental points and fitting result for undoped $SrTiO_3$ at 800 K (b) equivalent circuit for $SrTiO_3$ at 800 K.

As seen in Figure 8(a), at a higher temperature like 800 K, the Nyquist plot of undoped $SrTiO_3$ shows a well-defined semicircle, suggesting a dominant bulk conduction process. The experimental data (black squares) aligns closely with the fitted curve (red line), which shows the selected equivalent circuit describes the behaviour quite well.

The circuit used for 800 K fitting is as shown in Figure 8(b). At higher temperatures, the impedance response becomes more clear, and an additional contribution starts to appear as in Figure 8(a). So, an extra resistance element (R_2) is included in the equivalent circuit to account for this behaviour. The $R_1 \| CPE_1$ part is mainly associated with bulk conduction behaviour, while R_2 and CPE_2 represent additional interfacial or electrode-related contributions appearing at higher temperature. Although sometimes grain boundaries are modelled with separate RC elements, in this case, the fit does not explicitly resolve grain boundary effects.

Explanation of Circuit Elements

- $R_1 = 38.09\ \Omega$

  38.09 Ω represents the ionic resistance of the bulk material. Its relatively low value at 800 K suggests enhanced ionic mobility due to thermal activation, consistent with Arrhenius-type behavior.

- $R_2 = 2325\ \Omega$

The value of R_2 is relatively low, suggesting that increased temperature enhances charge carrier mobility, consistent with thermally activated conduction.

- CPE1 ($T = 1.26696\times10^{-6}$, $P = 0.58922$)

  The CPE1 shows the dielectric response of the material, so it shows how the material stores and releases charge in a non-ideal way. The P value of 0.589 indicates a highly non-ideal capacitive behavior, which may arise from structural inhomogeneity or a broad distribution of relaxation times due to defects or disorder.

- CPE2 ($T = 2.134\times10^{-7}$, $P = 0.80401$)

CPE2 is likely related to ion-blocking behaviour at the electrode interfaces, meaning some build-up or polarization happens where the ceramic touches the platinum contacts The T value indicates moderate capacitive strength, while the P value of ~0.80 shows that the behavior is reasonably close to an ideal capacitor but still affected by interfacial phenomena.

As shown in Figure 8(a) and (b), at 800 K, the undoped $SrTiO_3$ started showing more conductivity at high temperature. The Nyquist plot looked like a clean semicircle compared to 540 K. The R_1 dropped down to 38.09 Ω, which is a huge improvement from before. This shows that the overall resistance became much lower due to the temperature rise. CPE values stayed stable too, with value around 0.80.

4.2.2 Impedance spectra of Gd-doped samples

In this section the impedance spectra of undoped STO and Gd-doped STO based ceramics, $Sr_{0.85}Gd_{0.1}TiO_3$ and $Sr_{0.7}Gd_{0.2}TiO_3$ are analysed and compared as a function of temperature. For comparison purpose, impedance spectra at two different temperatures are considered.

Sample Name	Impedance Spectra-540 K	Equivalent Circuit
Undoped $SrTiO_3$	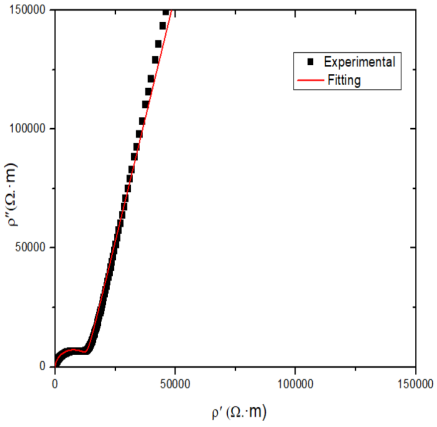 (a)	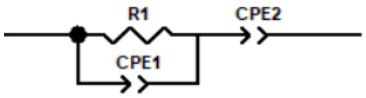 (b)

Element	Freedom	Value
R1	Free(+)	12302
CPE1-T	Free(+)	1.008E-9
CPE1-P	Free(+)	0.98948
CPE2-T	Free(+)	5.4934E-8
CPE2-P	Free(+)	0.84973

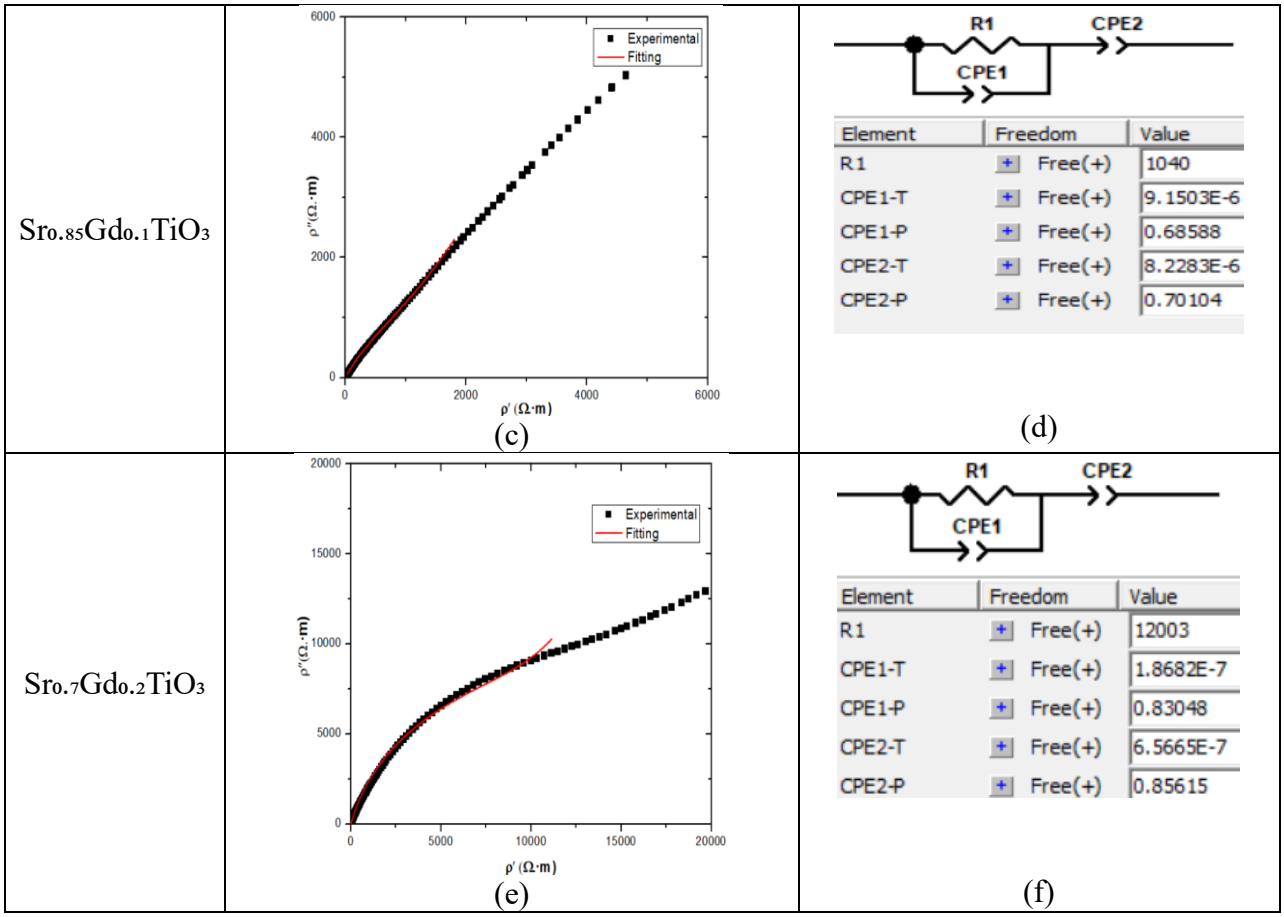

Fig. 9. Impedance Spectra and Equivalent Circuits at 540 K for undoped STO and Gd doped samples

As shown in figure 9(c) and (d), at 540 K, for the doped sample $Sr_{0.85}Gd_{0.1}TiO_3$, there was a drop in resistance when compared to undoped STO. The impedance plot barely rose above 6,000Ω total. The extracted R_1 was only 1,040 Ω, which is a big reduction compared to the undoped sample. That means doping with Gd improved the conductivity. Also, the CPE values were quite high in magnitude, and CPE-P value decreased to around 0.68–0.70, which is slightly less ideal. It maybe shows some more dispersion due to defect states introduced by Gd. But overall, the conductivity of this sample has improved compared to the undoped $SrTiO_3$.

Additionally, when it comes to $Sr_{0.7}Gd_{0.2}TiO_3$ sample, it had a bit different behavior. As in figure 9 (e) and (f), despite being more heavily doped (20% Gd), the R_1 jumped back up to 12,003 Ω, almost equal to the undoped $SrTiO_3$ sample. The impedance arc as shown in figure 9 (e) was broader than 10% Gd sample, and even curve fitting was slightly off at some points. This may be due to excessive dopant concentration, which can introduce defects or hinder charge transport. So basically, light doping helped conductivity, but heavier doping kind of reversed the gain *[3][10]*.

At a higher temperature of 800 K, as shown in Figure 10, a similar equivalent circuit to that used for the undoped $SrTiO_3$ sample at 800 K was found to fit the impedance data of the Gd-doped samples at the same temperature.

Sample Name	Impedance Spectra-800 K	Equivalent Circuit
Undoped $SrTiO_3$	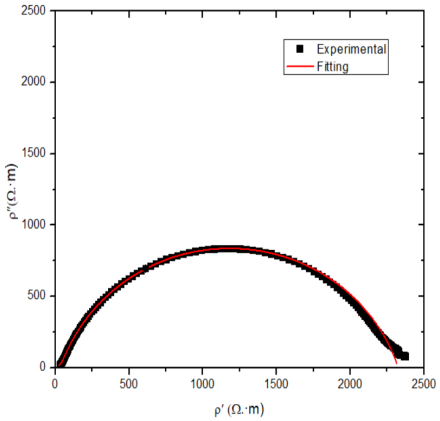 (a)	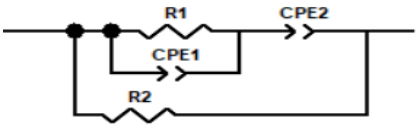 Element / Freedom / Value R1 Free(+) 38.09 CPE1-T Free(+) 1.2669E-6 CPE1-P Free(+) 0.58922 CPE2-T Free(+) 2.1342E-7 CPE2-P Free(+) 0.80401 R2 Free(+) 2325 (b)
$Sr_{0.85}Gd_{0.1}TiO_3$	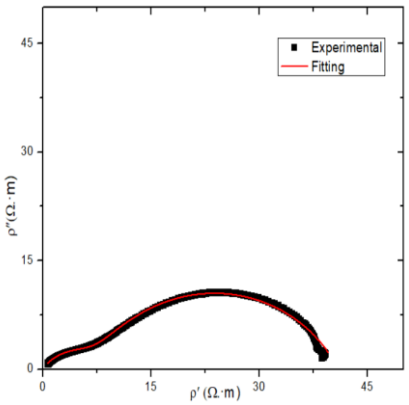 (c)	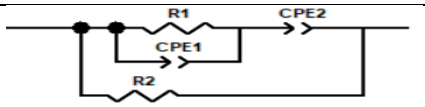 Element / Freedom / Value R1 Free(+) 8.47 CPE1-T Free(+) 3.524E-5 CPE1-P Free(+) 0.62698 CPE2-T Free(+) 9.2171E-5 CPE2-P Free(+) 0.70209 R2 Free(+) 40.96 (d)
$Sr_{0.7}Gd_{0.2}TiO_3$	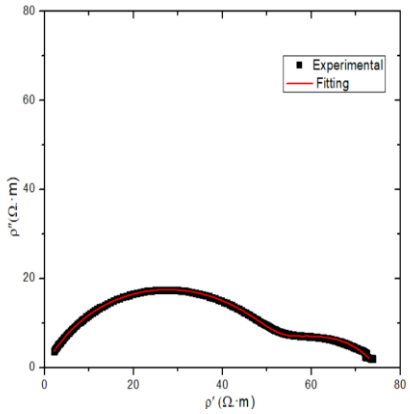 (e)	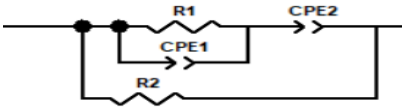 Element / Freedom / Value R1 Free(+) 146.9 CPE1-T Free(+) 1.6659E-6 CPE1-P Free(+) 0.73896 CPE2-T Free(+) 4.1243E-5 CPE2-P Free(+) 0.61585 R2 Free(+) 74.67 (f)

Fig. 10: Impedance Spectra and Equivalent Circuits at 800 K for undoped STO and Gd doped samples

At 800 K, the Gd-doped samples show improved conductivity when compared to 540 K. Compared to the undoped $SrTiO_3$ sample at the same temperature, the Gd-doped $Sr_{0.85}Gd_{0.1}TiO_3$ sample exhibit much lower resistance, indicating enhanced conductivity. That is, R_1 is as low as 8.47 Ω. The plot looked very flattened and low impedance. R_2 stayed at 40.96 Ω. However, the CPE values started dropping a bit, suggesting more non-ideal capacitive

behavior, probably due to defects from dopant ions. But even so, the conduction remained strongest here.

Furthermore, the $Sr_{0.7}Gd_{0.2}TiO_3$ sample again did not perform as expected. The R_1 increased to 146.9 Ω, which is even higher than the undoped $SrTiO_3$ sample at the same temperature (38.09 Ω), and significantly higher than the 10% Gd sample. R_2 was around 74.67 Ω. This suggests that increasing Gd concentration beyond a certain level may start to reduce conductivity possibly due to clustering or trapping defects forming *[3][10].*Also, the CPE-P dropped to 0.61 range which shows some more non-ideal effects. So overall, higher Gd content does not improve conductivity and may negatively affect the transport properties.

Lastly, compared to YSZ, which shows a clear semicircle and mainly ionic conduction, both undoped and Gd-doped $SrTiO_3$ samples show more complex behaviour. The Gd-doped sample with lower concentration shows better conductivity, but the behaviour is still not like YSZ. Also, increasing the Gd content further does not improve the conductivity and can even make it worse.

4.2.3 Impedance spectra of La-doped samples

In this section, the impedance spectra La-doped STO based ceramics are analysed and compared. To be consistent with the previous section, consider only the impedance spectra of two different temperatures, 540 K and 800 K. The samples that were measured are $Sr_{0.85}La_{0.1}TiO_3$, $Sr_{0.7}La_{0.2}TiO_3$, $Sr_{0.75}La_{0.25}TiO_3$, $Sr_{0.65}La_{0.35}TiO_3$ and $Sr_{0.55}La_{0.3}TiO_3$.

To explain the behaviour of impedance spectra, $Sr_{0.55}La_{0.3}TiO_3$ sample is discussed in detail while keeping the summary of the other compositions. The figure 11(a) and (b) shows the experimental points and fitting result for $Sr_{0.55}La_{0.3}TiO_3$ at 540 K and its equivalent circuit.

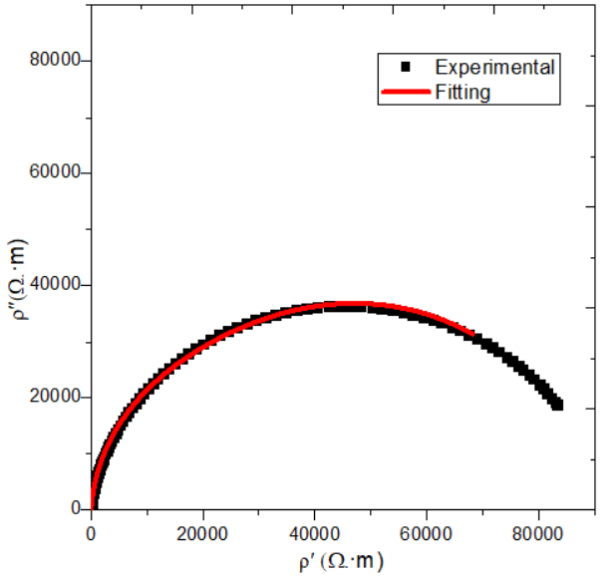

(a)

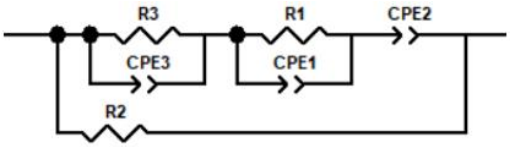

Element	Freedom	Value
R3	Free(+)	9.466
CPE3-T	Free(+)	8.421E-9
CPE3-P	Fixed	1
R1	Free(+)	10549
CPE1-T	Free(+)	3.9321E-8
CPE1-P	Fixed	1
CPE2-T	Free(+)	1.7688E-8
CPE2-P	Free(+)	0.94748
R2	Free(+)	88334

(b)

Fig. 11 (a): Experimental points and fitting result for $Sr_{0.55}La_{0.3}TiO_3$ at 540 K (b) equivalent circuit for $Sr_{0.55}La_{0.3}TiO_3$ at 540 K.

The Nyquist plot of $Sr_{0.55}La_{0.3}TiO_3$ shows a depressed arc instead of a proper semicircle, which indicates non-ideal behaviour. This can be mainly due to overlapping effects from bulk, grain boundary and also electrode polarization at lower frequencies *[27]*.

The fitting curve matches well with the experimental data, so the chosen equivalent circuit seems to describe the impedance behaviour reasonably well. Similar to the udoped and Gd doped $SrTiO_3$ sample, the circuit includes resistive and constant phase elements, which means the overall conduction mechanism is similar, but obviously the values are different.

Compared to the undoped $SrTiO_3$ at the same temperature, the La-doped sample shows lower resistance, which means the conductivity has improved due to doping. But still, the nature of the arc shows that non-ideal behaviour and can be due to defect-related effects *[4]*.

Additionally, the figure 12(a) and (b) shows the experimental points and fitting result for $Sr_{0.55}La_{0.3}TiO_3$ at 800 K and its equivalent circuit.

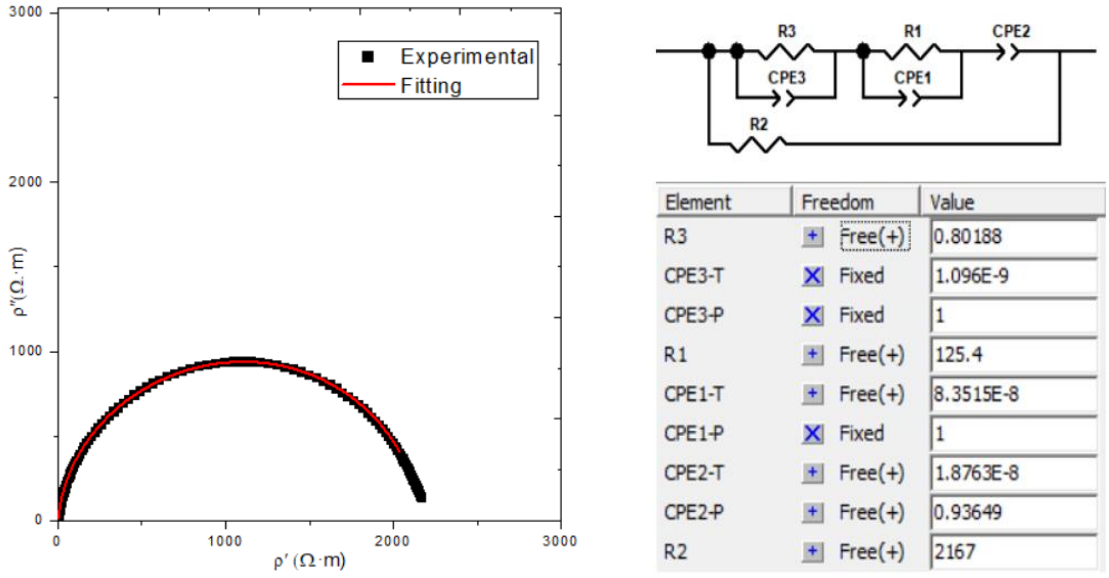

(a) (b)

Fig. 12(a): Experimental points and fitting result for $Sr_{0.55}La_{0.3}TiO_3$ at 800 K (b) equivalent circuit for $Sr_{0.55}La_{0.3}TiO_3$ at 800 K.

At a higher temperature like 800 K, the impedance spectrum of $Sr_{0.55}La_{0.3}TiO_3$ shows a further decrease in resistance, which is expected due to thermally activated charge transport. The Nyquist plot becomes more compressed, indicating better conductivity compared to lower temperature *[27]*.

As mentioned, the same equivalent circuit was able to fit the data at this temperature as well, which shows that the main conduction processes are still the same, only their contribution changes with temperature. The presence of a single semicircular arc indicates that the bulk and grain boundary contributions are not clearly separated but appear as an overlapping response, which is commonly observed in doped $SrTiO_3$ systems *[4]*.

Overall, the same equivalent circuit was used for the La-doped samples because the general shape of the impedance spectra remained similar across the temperature range. With increasing temperature, the resistance decreases and the semicircle becomes smaller, showing a thermally activated conduction behaviour. The spectra consistently show a single depressed semicircle, suggesting overlapping contributions from bulk and grain boundary regions, which is a common feature in doped $SrTiO_3$ ceramics *[4].*

After fitting the impedance spectra of all La-doped samples, the extracted resistance values at 540 K and 800 K are summarized in Table 1.

Sample	**540 K**			**800 K**		
	R_3(Ω.m)	R_1(Ω.m)	R_2(Ω.m)	R_3(Ω.m)	R_1(Ω.m)	R_2(Ω.m)
$Sr_{0.85}La_{0.1}TiO_3$	94.3	2.23×10^5	N/A	1.9	38.8	67.47
$Sr_{0.7}La_{0.2}TiO_3$	63.99	26384	43302	0.417	12.16	9.017
$Sr_{0.75}La_{0.25}TiO_3$	334.4	3,492.50	26,235	11.9	79.8	96.618
$Sr_{0.55}La_{0.3}TiO_3$	9.4	10549	88334	0.8	125.4	2167
$Sr_{0.65}La_{0.35}TiO_3$	741.7	9819	24855	9.955	31.59	75.15

Table 1: Summary of fitted resistance parameters for La-doped $SrTiO_3$ samples at 540 K and 800 K.

In general, all the samples show a decrease in resistance with increase in temperature, which indicates thermally activated conduction behaviour. However, the resistance values are not changing in a perfectly linear way with increasing La concentration. Some samples show lower resistance values while others show comparatively higher values, suggesting that the impedance response is influenced not only by dopant concentration, but also by factors such as grain boundary contribution, defect distribution and microstructural changes within the ceramic *[6].*

From the table, it can also be observed that the semicircular arc becomes smaller at higher temperature for all compositions, which aligns with the Nyquist plots discussed earlier. The lower resistance values at 800 K indicate improved conductivity at elevated temperature. At the same time, the fitting parameters suggest that the conduction processes are still overlapping in nature, since a single depressed semicircle is mainly observed in most of the spectra. Similar behaviour is commonly seen in doped $SrTiO_3$ ceramics where both bulk and grain boundary effects contribute together to the overall impedance response *[23].*

Although La doping generally improves the conductivity of $SrTiO_3$ compared to the undoped sample, the results show that increasing the La content does not always continuously improve the electrical behaviour. For example, the $Sr_{0.7}La_{0.2}TiO_3$ sample shows comparatively lower resistance values at 800 K than some higher La-doped compositions such as $Sr_{0.65}La_{0.35}TiO_3$. This indicates that the change in electrical behaviour with La concentration is not completely linear. This shows that there may be an optimum range of doping where the conductivity improvement becomes more effective, while excessive doping can introduce additional defect-related or microstructural effects that influence the impedance response *[7].*

Compared to the undoped $SrTiO_3$ sample, the La-doped samples generally show lower impedance values and improved conductivity, especially at higher temperatures. However, as mentioned above, the improvement does not increase continuously with increasing La concentration. From the table, $Sr_{0.7}La_{0.2}TiO_3$ shows lower resistance values at 800 K compared to some higher La-doped samples, so the behaviour is not fully linear with doping amount.

Additionally, when compared to YSZ, the impedance response of La-doped $SrTiO_3$ is more complex. YSZ is used as a reference ionic conductor, while La-doped $SrTiO_3$ shows depressed semicircular arcs and overlapping contributions from different processes. This shows that the La-doped samples are not behaving like pure ionic conductors, but have mixed ionic–electronic type behaviour *[14] [25]*.

Overall, the impedance spectra analysis shows that La doping changes the electrical behaviour of $SrTiO_3$ and improves conductivity compared to the undoped sample. But higher La concentration does not always give better transport behaviour, which may be due to defect-related effects, grain boundary contribution or microstructural changes in the ceramic *[4] [25]*.

4.2.4 Impedance spectra of Nd-doped samples

In this section, neodymium (Nd)-doped $SrTiO_3$ ceramics was investigated to study the effect of Nd substitution on the impedance behaviour of $SrTiO_3$. In this section, two Nd-doped compositions, $Sr_{0.85}Nd_{0.1}TiO_3$ and $Sr_{0.7}Nd_{0.2}TiO_3$, are analysed and compared with the undoped $SrTiO_3$ sample. Similar to the La-doped samples, the same equivalent circuit was used for fitting since the Nyquist plots showed a similar depressed semicircular response.

For consistency with the previous sections, the impedance behaviour is discussed mainly at 540 K and 800 K. These two temperatures help to compare the low-temperature and high-temperature response without repeating the full fitting explanation for every measured temperature.

The impedance spectra and equivalent circuit fitting parameters of the undoped $SrTiO_3$, $Sr_{0.85}Nd_{0.1}TiO_3$ and $Sr_{0.7}Nd_{0.2}TiO_3$ samples at 540 K are shown in figure 13. Compared to the undoped $SrTiO_3$ sample, both Nd-doped samples showed much lower impedance response, which indicates enhanced conductivity after Nd doping.

Between the two Nd-doped samples, $Sr_{0.7}Nd_{0.2}TiO_3$ showed a much smaller semicircle and lower resistance values compared to $Sr_{0.85}Nd_{0.1}TiO_3$. This suggests that increasing Nd doping concentration improved the charge transport at 540 K. Similar changes in transport behaviour after Nd substitution have also been reported in Nd-doped $SrTiO_3$ systems *[8]*.

Sample Name	Impedance Spectra-540 K	Equivalent Circuit

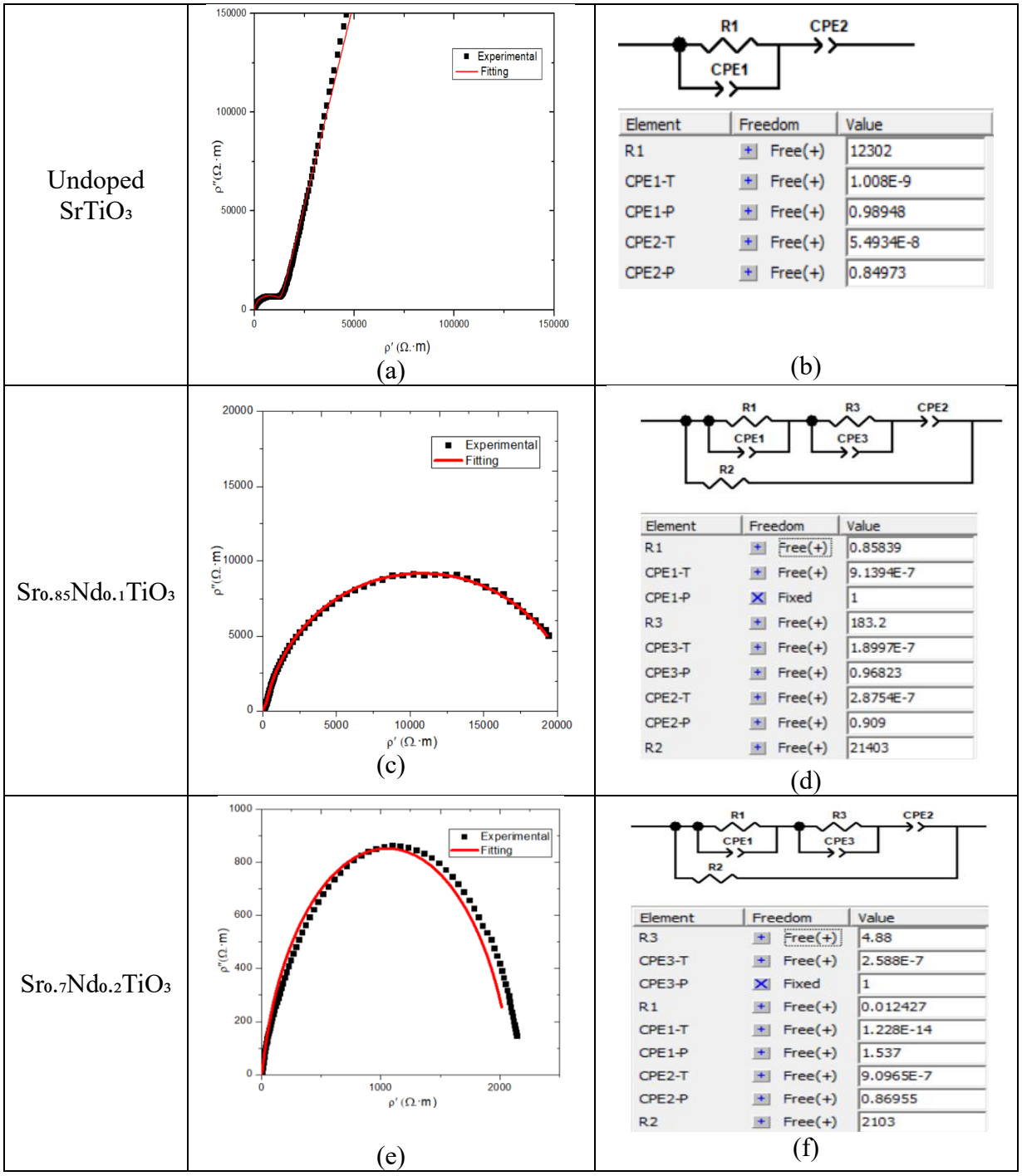

Fig. 13: Impedance spectra and equivalent circuit fitting parameters of undoped $SrTiO_3$, $Sr_{0.85}Nd_{0.1}TiO_3$ and $Sr_{0.7}Nd_{0.2}TiO_3$ samples at 540 K.

The impedance spectra and equivalent circuit fitting parameters of the undoped $SrTiO_3$, $Sr_{0.85}Nd_{0.1}TiO_3$ and $Sr_{0.7}Nd_{0.2}TiO_3$ samples at 800 K are shown in figure 14. Compared to the behaviour at 540 K, all the samples showed a strong reduction in impedance at higher temperature. The semicircular arcs became much smaller and more compressed, indicating improved conductivity due to thermally activated charge transport. The fitting curves showed good alignment with the experimental data.

Fig. 14: Impedance spectra and equivalent circuit fitting parameters of undoped $SrTiO_3$, $Sr_{0.85}Nd_{0.1}TiO_3$ and $Sr_{0.7}Nd_{0.2}TiO_3$ samples at 800 K.

Among the Nd-doped samples, $Sr_{0.7}Nd_{0.2}TiO_3$ showed the lowest impedance response and smallest resistance values at 800 K. When compared to the undoped $SrTiO_3$ sample, both Nd-doped compositions showed significantly improved conductivity at higher temperature. The

Sample Name	Impedance Spectra-800 K	Equivalent Circuit
Undoped $SrTiO_3$	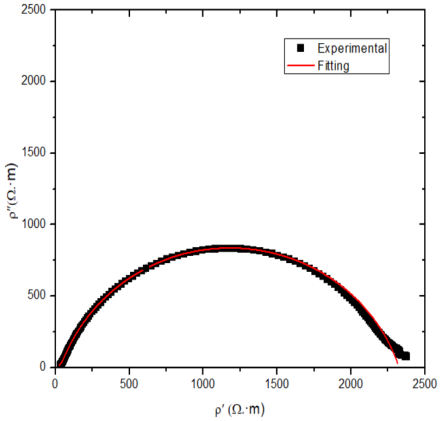 (a)	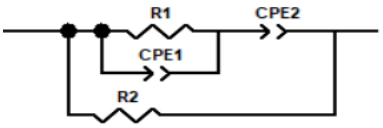 (b)
$Sr_{0.85}Nd_{0.1}TiO_3$	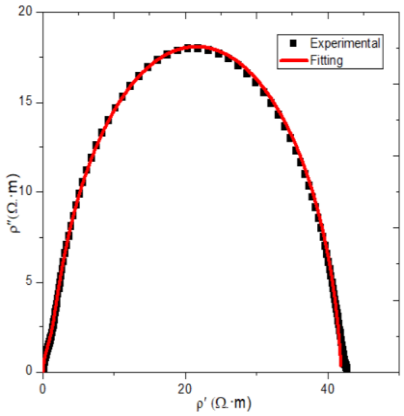 (c)	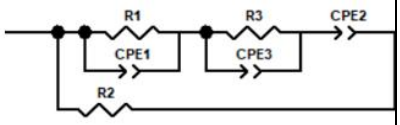 (d)
$Sr_{0.7}Nd_{0.2}TiO_3$	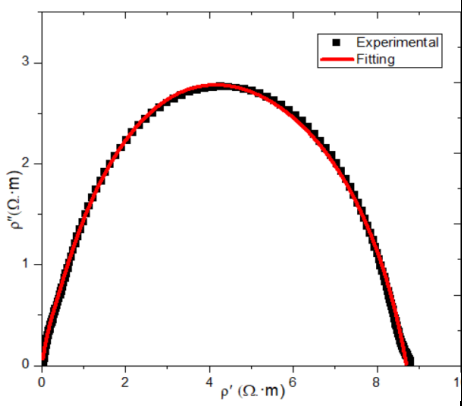 (e)	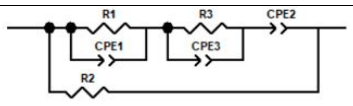 (f)

Element	Freedom	Value
R1	Free(+)	38.09
CPE1-T	Free(+)	1.2669E-6
CPE1-P	Free(+)	0.58922
CPE2-T	Free(+)	2.1342E-7
CPE2-P	Free(+)	0.80401
R2	Free(+)	2325

Element	Freedom	Value
R3	Free(+)	0.029536
CPE3-T	Free(+)	4.641E-9
CPE3-P	Free(+)	0.94267
R1	Free(+)	1.263
CPE1-T	Free(+)	3.4221E-7
CPE1-P	Free(+)	0.91892
CPE2-T	Free(+)	3.2331E-7
CPE2-P	Free(+)	0.92711
R2	Free(+)	41.88

Element	Freedom	Value
R3	Free(+)	0.10917
CPE3-T	Free(+)	6.1229E-7
CPE3-P	Fixed	1
R1	Free(+)	1.157
CPE1-T	Free(+)	2.2368E-6
CPE1-P	Fixed	1
CPE2-T	Free(+)	7.5699E-6
CPE2-P	Free(+)	0.74947
R2	Free(+)	8.703

results suggest that Nd substitution strongly influences the transport behaviour of $SrTiO_3$ and reduces the overall resistance of the material. Similar improvement in electrical transport behaviour after Nd doping has also been observed in Nd-doped $SrTiO_3$ systems *[8]*.

Compared to YSZ, the impedance response of the Nd-doped samples appeared more compressed and showed overlapping contributions from different conduction processes. This indicates that the Nd-doped $SrTiO_3$ samples do not behave like pure ionic conductors, but instead show mixed conduction behaviour similar to the previously discussed Gd- and La-doped samples.

4.3 Temperature Dependencies of Conductivity

This section discusses the temperature dependence of ionic and electronic conductivity for all investigated samples. Arrhenius plots were used to estimate the activation energy of the conduction processes by plotting the logarithmic conductivity against the inverse temperature. From these graphs, the activation energies for both ionic (grain and grain boundary) and electronic conductivities of all samples were calculated and analyse how doping impacts the electrical properties of $SrTiO_3$.

As mentioned above, the Arrhenius is widely used in analysing semiconducting oxides. The basic idea is that as temperature increases, more charge carriers become thermally activated, allowing for increased conductivity. This behavior is typically described by the Arrhenius equation:

$$\sigma = \sigma_0 \cdot \exp(-\Delta E / kT) \qquad (5)$$

where σ_0 is the pre-exponential factor, ΔE is the activation energy for charge transport, k is Boltzmann's constant, and T is absolute temperature.

Taking the logarithm of both sides gives a linear relationship:

$$\log \sigma = \log \sigma_0 - (\Delta E / (k \ln 10)) \cdot (1/T) \qquad (6)$$

This means that if $\log(\sigma)$ vs 1/T is plotted (or equivalently $1/\rho$ vs 1000/T, since resistivity and conductivity are inversely related), the data should form a straight line, and the slope of that line is directly related to the activation energy.

After plotting, linear fitting of the graph was performed in Origin software to extract the slope value. This slope allows to calculate the activation energy (ΔE) for conduction using the simplified relationship:

$$\Delta E \approx -0.2 \times \text{slope [eV]} \qquad (7)$$

This 0.2 factor arises from substituting fundamental constants into the Arrhenius-derived expression and converting from Joules to electron volts.

4.3.1 Conductivity of undoped $SrTiO_3$

Figure 15 shows the temperature dependence of bulk ionic conductivity, grain boundary ionic conductivity, total ionic conductivity, and electronic conductivity of undoped $SrTiO_3$ plotted as log σ versus 1000/T. All conductivity components increase with increasing temperature, indicating thermally activated charge transport. The nearly linear behaviour of log σ with 1000/T suggests that the conduction processes in $SrTiO_3$ follow Arrhenius-type behaviour, which is typical for oxide ceramics.

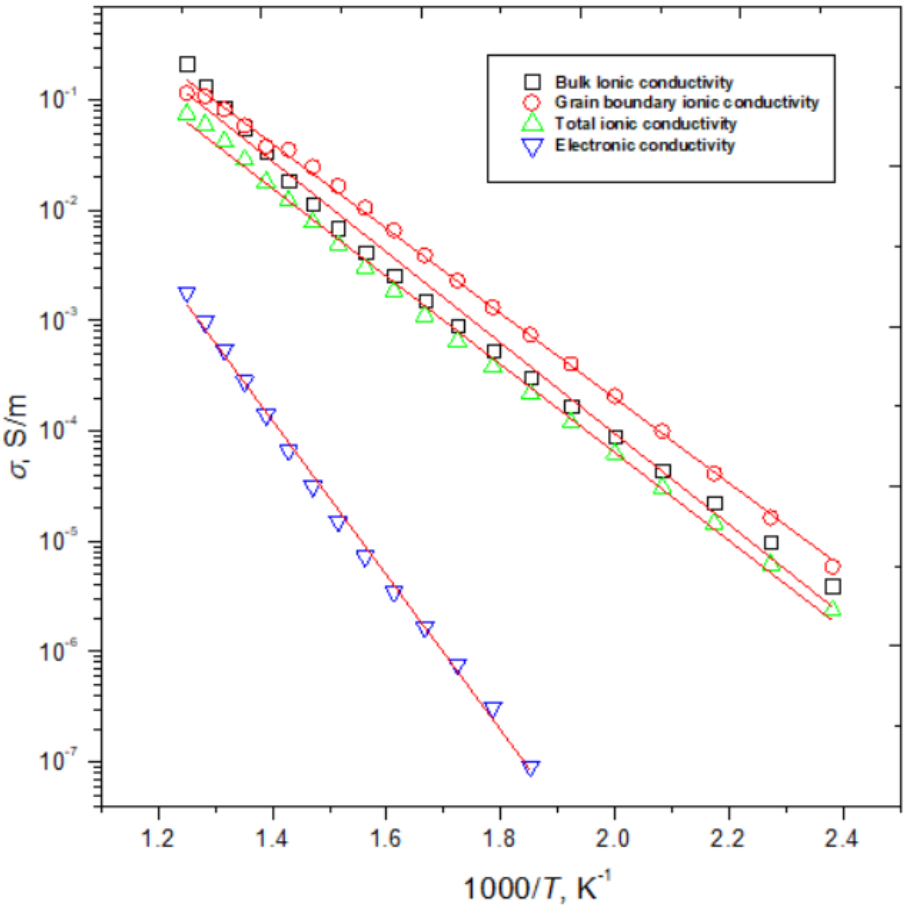

Fig. 15: Conductivity vs. Inverse Temperature Graph for undoped $SrTiO_3$

The bulk ionic conductivity is higher than the grain boundary ionic conductivity across the entire temperature range. This indicates that ionic transport within the grain interior is relatively easier, while grain boundaries act as more resistive regions. The higher resistance at grain boundaries can be attributed to structural disorder and defect accumulation, which hinder the movement of oxygen ions across these regions.

The total ionic conductivity lies closer to the grain boundary ionic conductivity than to the bulk ionic conductivity. This shows that the overall ionic conduction in $SrTiO_3$ ceramics is mainly controlled by the grain boundaries rather than by the grain interior. Even though the bulk grains exhibit higher ionic conductivity, the resistive nature of grain boundaries limits or reduces the effective ionic transport through the sample. Such grain-boundary-controlled ionic conduction is commonly observed in polycrystalline $SrTiO_3$ ceramics *[13]*.

The electronic conductivity of $SrTiO_3$ is several orders of magnitude lower than the ionic conductivity over the entire temperature range. Although it increases with temperature, its magnitude remains much smaller compared to the ionic contributions. This confirms that undoped $SrTiO_3$ behaves mainly as an ionic conductor under the present experimental conditions.

4.3.2 Bulk ionic conductivity of STO and doped STO

The bulk ionic conductivity of undoped $SrTiO_3$ and doped $SrTiO_3$ samples is shown in the Figure 16.

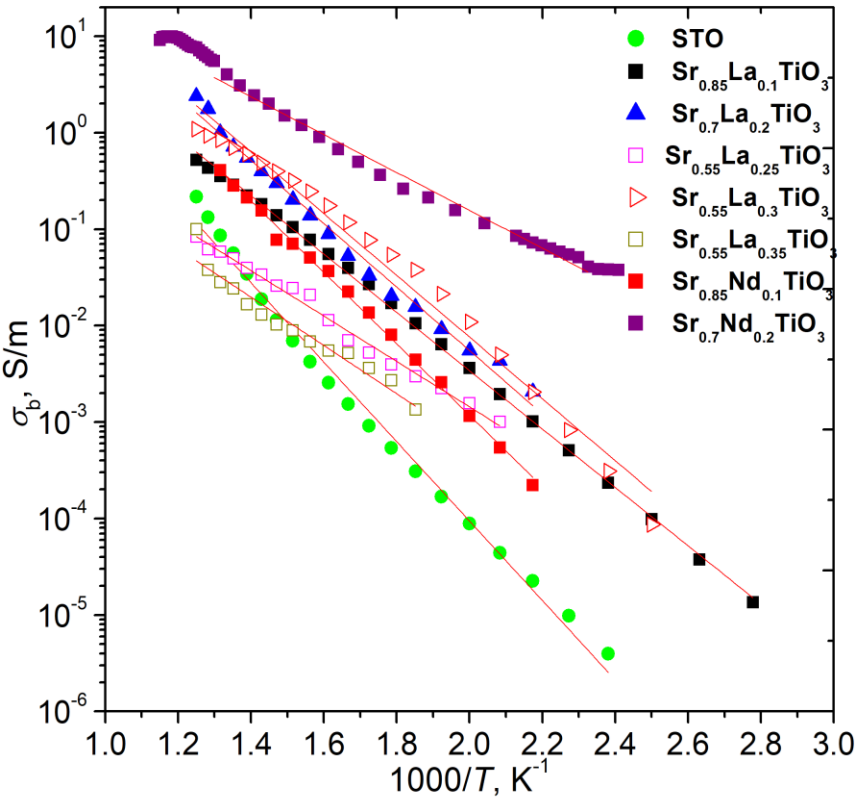

Fig. 16: Bulk Ionic Conductivity vs. Inverse Temperature Graph

Compared to the undoped STO sample, most of the doped samples showed higher bulk ionic conductivity over the measured temperature range. Among all the samples, $Sr_{0.7}Nd_{0.2}TiO_3$ showed the highest bulk ionic conductivity, while the undoped STO sample showed the lowest conductivity. This indicates that Nd doping has a noticeable effect on the ionic transport behaviour of $SrTiO_3$. Similar behaviour has also been reported in doped $SrTiO_3$ systems due to oxygen vacancy related transport and defect formation *[8]*.

The La-doped samples also showed improved conductivity compared to the undoped STO sample, but the behaviour was not exactly same for all compositions. Some of the curves were

very close to each other, while some compositions showed only small improvement. This shows that increasing La concentration did not always improve the bulk ionic conductivity in a linear way. Overall, the doped samples showed better bulk ionic transport behaviour compared to the undoped STO sample.

4.3.3. Total Ionic conductivity of STO and doped STO

The temperature dependence of total ionic conductivity for undoped STO and doped STO samples is shown in Figure 17.

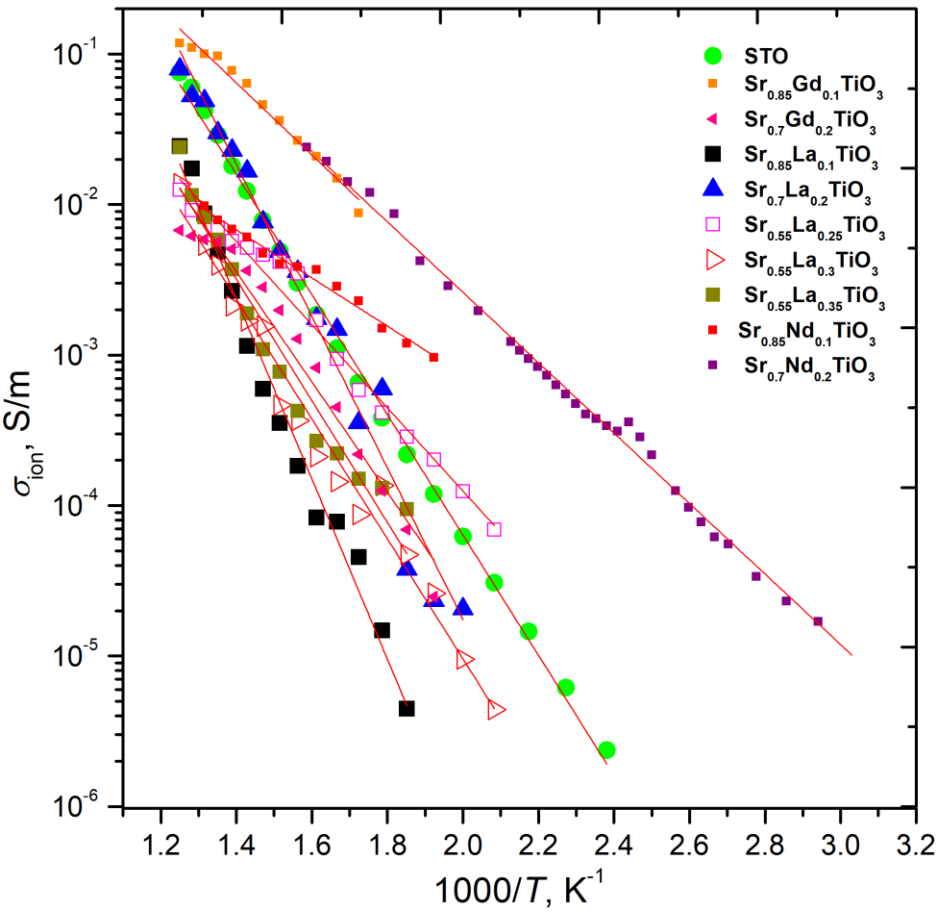

Fig. 17: Total Ionic Conductivity vs. Inverse Temperature Graph

Compared to the bulk ionic conductivity graph, the difference between the samples can be seen more clearly in this graph. For most of the samples, the conductivity became higher as the temperature increased.

From all the investigated samples, $Sr_{0.7}Nd_{0.2}TiO_3$ showed the highest total ionic conductivity in most parts of the graph. The Gd-doped samples also showed improved conductivity, especially $Sr_{0.85}Gd_{0.1}TiO_3$. However, the conductivity reduced again for $Sr_{0.7}Gd_{0.2}TiO_3$, showing that increasing the Gd concentration further did not improve the ionic transport behaviour. This same trend was also observed earlier in the impedance spectra section.

For the La-doped samples, the conductivity behaviour was not same for all compositions. Some samples showed conductivity values close to or lower than the undoped STO sample. This shows that the total ionic conductivity does not depend only on the dopant concentration. Grain boundary effects and the microstructure of the samples also affects the ionic transport behaviour. Overall, each doped sample showed slightly different conductivity behaviour *[8]*.

4.3.4. Electronic conductivity of STO and doped STO

Figure 18 shows the temperature dependence of electronic conductivity for $SrTiO_3$ and doped $SrTiO_3$ samples. Compared to the undoped STO sample, most of the doped samples showed higher electronic conductivity. The difference between the samples can also be seen more clearly in this graph. For many of the samples, the conductivity became higher at higher temperatures.

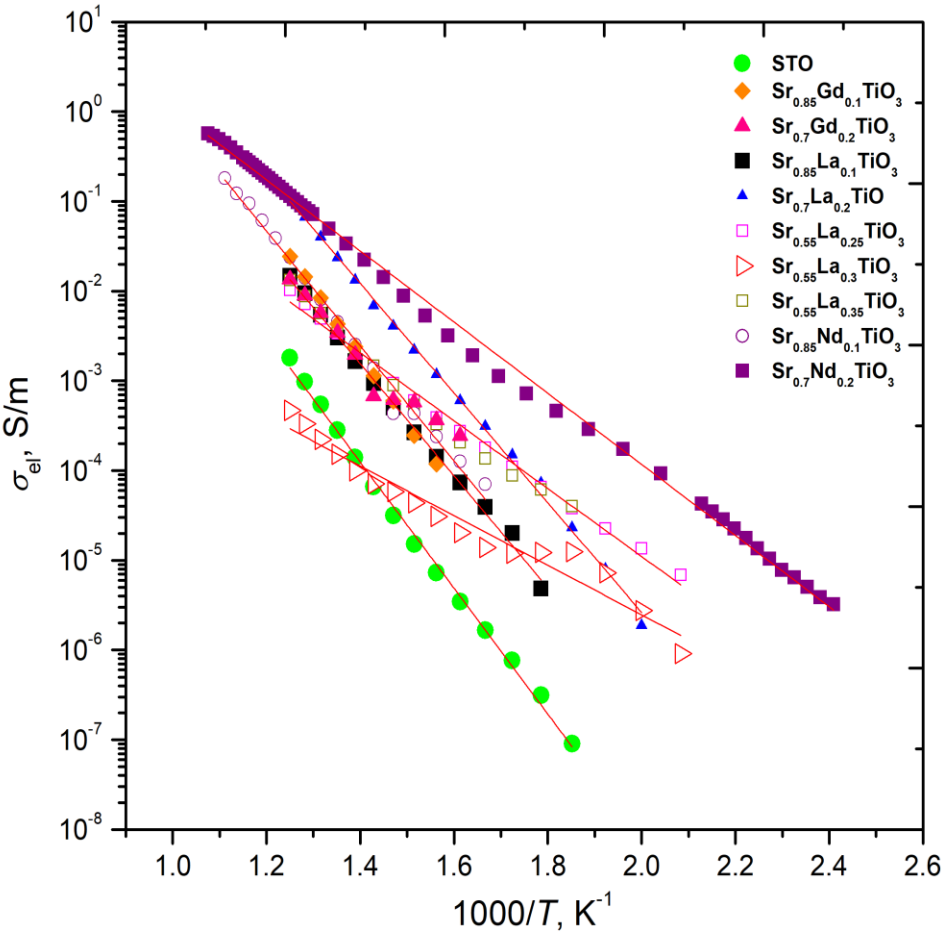

Fig. 18: Electronic Conductivity Vs Inverse Temperature Graph

Among all the samples, $Sr_{0.7}Nd_{0.2}TiO_3$ showed the highest electronic conductivity over most parts of the measured temperature range. $Sr_{0.85}Nd_{0.1}TiO_3$ also showed higher conductivity compared to the undoped STO sample and several La-doped compositions. The Gd-doped samples also showed improved electronic conductivity compared to the undoped STO sample.

In the case of La-doped samples, the conductivity behaviour was different for different compositions. Some samples showed only small improvement, while some remained close to the undoped STO behaviour in certain temperature regions. This shows that the electronic conductivity did not change in the same way for all samples. Different dopants and different doping amounts affected the electronic transport behaviour differently *[8]*.

4.3.5. Activation Energy Analysis

The activation energy values obtained from the Arrhenius plots for bulk ionic, total ionic and electronic conductivity are summarized in Table 2.

Activation Energy			
Sample composition	**ΔE_Ionic bulk (eV)**	**ΔE_Ionic total (eV)**	**ΔE_electronic (eV)**
$SrTiO_3$	0.82	0.80	1.40
$Sr_{0.85}Gd_{0.1}TiO_3$	N/A	0.48	1.49
$Sr_{0.7}Gd_{0.2}TiO_3$	N/A	0.73	0.98
$Sr_{0.85}La_{0.1}TiO_3$	0.60	1.20	1.25
$Sr_{0.7}La_{0.2}TiO_3$	0.66	1.01	1.22
$Sr_{0.75}La_{0.25}TiO_3$	0.47	0.55	0.76
$Sr_{0.55}La_{0.3}TiO_3$	0.64	0.80	0.55
$Sr_{0.65}La_{0.35}TiO_3$	0.50	0.94	0.86
$Sr_{0.85}Nd_{0.1}TiO_3$	0.74	0.32	1.28
$Sr_{0.7}Nd_{0.2}TiO_3$	0.44	0.47	0.80

Table 2: Activation energy values for ionic and electronic conduction.

In general, the activation energy values changed after doping, showing that the dopants influenced the transport behaviour of $SrTiO_3$ in different ways.

For bulk ionic conductivity, the activation energy values of many doped samples became lower than the undoped STO sample. The undoped STO sample gave a value of 0.82 eV. Some doped samples such as $Sr_{0.7}Nd_{0.2}TiO_3$, $Sr_{0.75}La_{0.25}TiO_3$ and $Sr_{0.65}La_{0.35}TiO_3$ gave smaller activation energy values. This indicates that ionic transport became easier in these samples after doping. However, all samples did not follow exactly the same trend.

For total ionic conductivity, the activation energy values again changed from sample to sample. Smaller values were seen for $Sr_{0.85}Nd_{0.1}TiO_3$, $Sr_{0.7}Nd_{0.2}TiO_3$ and $Sr_{0.85}Gd_{0.1}TiO_3$ compared to several other compositions. This indicates that some doped samples needed less energy for ionic transport. Grain boundary contribution and sample microstructure may also influence this behaviour.

For electronic conductivity, $Sr_{0.85}Gd_{0.1}TiO_3$ gave the highest activation energy value of 1.49 eV, which was slightly higher than the STO sample. Some other doped samples such as $Sr_{0.55}La_{0.3}TiO_3$, $Sr_{0.75}La_{0.25}TiO_3$ and $Sr_{0.7}Nd_{0.2}TiO_3$ showed smaller activation energy values. From the overall results, it can be seen that the conductivity behaviour changed depending on the dopant and the doping amount *[8]*.

4.4 Dielectric Relaxation Behaviour of $Sr_{0.7}Nd_{0.2}TiO_3$

The dielectric relaxation behaviour was analysed for $Sr_{0.7}Nd_{0.2}TiO_3$. This sample was selected because it had already been studied earlier in the laboratory, where a transition-like or lattice-related change was observed. Therefore, the available dielectric data for this composition were used to examine whether its relaxation behaviour also shows changes with temperature. In addition, this sample showed comparatively good electrical behaviour in the conductivity analysis, which made it suitable for further dielectric relaxation study.

Dielectric relaxation is useful to see how the sample responds when frequency and temperature are changed. In $SrTiO_3$-based materials, the dielectric response can be influenced by defects, oxygen vacancies, local polar regions and movement of charge carriers. Because of this, the response may not always come from one simple process. In some cases, more than one relaxation process can be seen, and the Arrhenius plot may also deviate from a single straight-line behaviour over the whole temperature range. Similar complex relaxation behaviour has been reported earlier for $SrTiO_3$ ceramics and doped $SrTiO_3$ systems *[17] [19]*.

For $Sr_{0.7}Nd_{0.2}TiO_3$, two relaxation times were obtained from the dielectric data and represented as τ_1 and τ_2. When these values were plotted with temperature, both relaxation times showed different changes. Therefore, τ_1 and τ_2 are discussed separately in the following sections, so that the relaxation behaviour can be compared more clearly.

4.4.1 Dielectric Relaxation Spectra

As mentioned in the previous section, the dielectric relaxation data for $Sr_{0.7}Nd_{0.2}TiO_3$ were obtained from previously recorded laboratory measurements and were used here for analysis. The available data covered a wide temperature range from 273 K to 930 K. Since many temperature curves were present, only selected temperatures are shown in Figure 19 and Figure 20 to make the spectra easier to read.

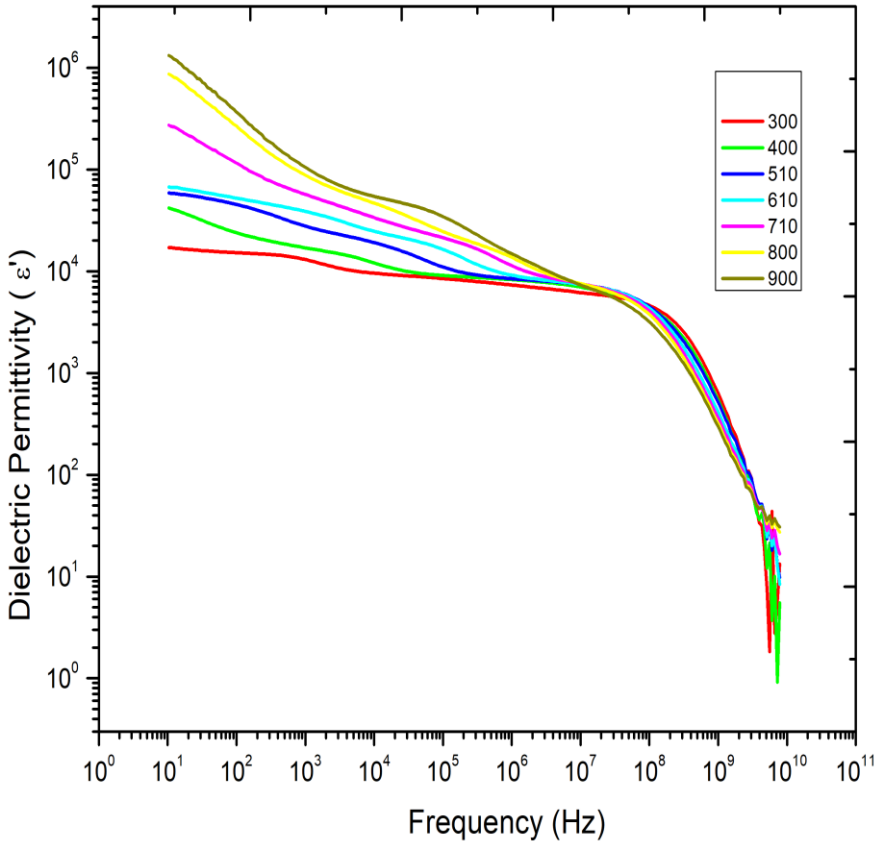

Fig. 19: Frequency dependence of dielectric permittivity ε′ for $Sr_{0.7}Nd_{0.2}TiO_3$ at selected temperatures

Figure 19 shows the frequency dependence of dielectric permittivity ε′ for $Sr_{0.7}Nd_{0.2}TiO_3$. From the graph, it can be seen that ε′ is high at lower frequencies and decreases when the frequency increases. This type of behaviour is common in dielectric materials because polarization processes are able to follow the applied field better at low frequency, while at high frequency they cannot respond in the same way. Similar frequency-dependent dielectric response has also been discussed in $SrTiO_3$-based ceramics *[17]*.

At higher temperatures, the low-frequency permittivity becomes much larger. This may be connected with stronger charge accumulation, defect-related polarization, or conduction contribution at lower frequencies. In $SrTiO_3$-based materials, defects, oxygen vacancies and local polar regions can strongly affect dielectric behaviour, so this kind of temperature-dependent change is expected *[17] [18]*.

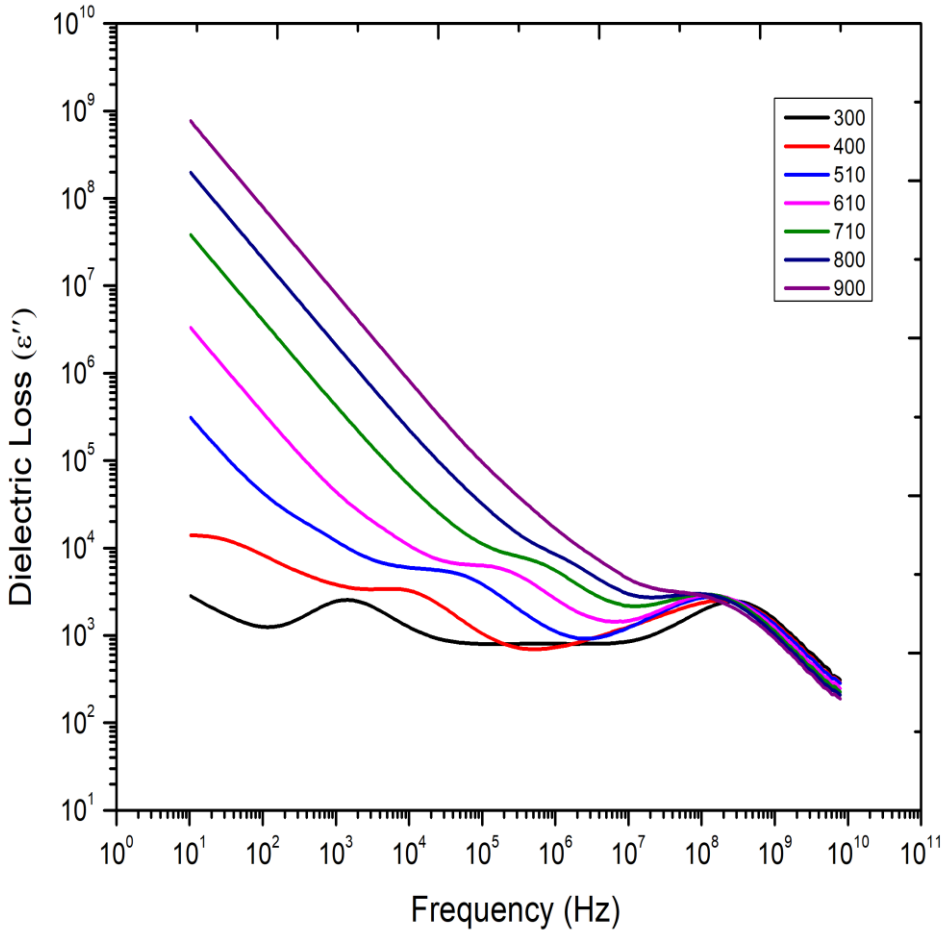

Fig. 20: Frequency dependence of dielectric loss ε″ for $Sr_{0.7}Nd_{0.2}TiO_3$ at selected temperatures.

Figure 20 shows how the dielectric loss ε″ changes with frequency for the same sample. From the graph, the loss is higher at the low-frequency side, and this increase becomes more clear when the temperature is higher. This shows that loss processes become stronger when temperature increases. In the middle and high frequency range, broad relaxation-type features can be noticed instead of one sharp peak. This means that the dielectric response is not controlled by only one simple process.

The dielectric loss spectra are important for relaxation analysis because relaxation processes are usually seen from peaks or broad changes in ε″. From the available dielectric data, two relaxation contributions were separated and later represented as τ_1 and τ_2. The presence of more than one relaxation process has also been reported in $SrTiO_3$ ceramics, where relaxation behaviour was related to defect and local polarization effects *[17]*. Similar defect-related dielectric relaxation has also been reported in rare-earth substituted $SrTiO_3$ ceramics *[18]*.

4.4.2 Relaxation Time Analysis

Once the ε′ and ε″ spectra were plotted, the relaxation time analysis was carried out for $Sr_{0.7}Nd_{0.2}TiO_3$. Relaxation time shows how much time the sample takes to respond to the changing electric field. When this value is lower, the response is faster, and when it is higher, the response is slower.

For this part, the available dielectric data were fitted using a relaxation model. Both the real part of permittivity ε′ and the imaginary part ε″ were included in the fitting. A representative fitting result at 320 K is shown in Figure 21. In this figure, the experimental ε′ and ε″ curves are shown together with the fitted curves. Since the fitted curves follow the main shape of the experimental data, the fitting parameters were used to obtain the relaxation times.

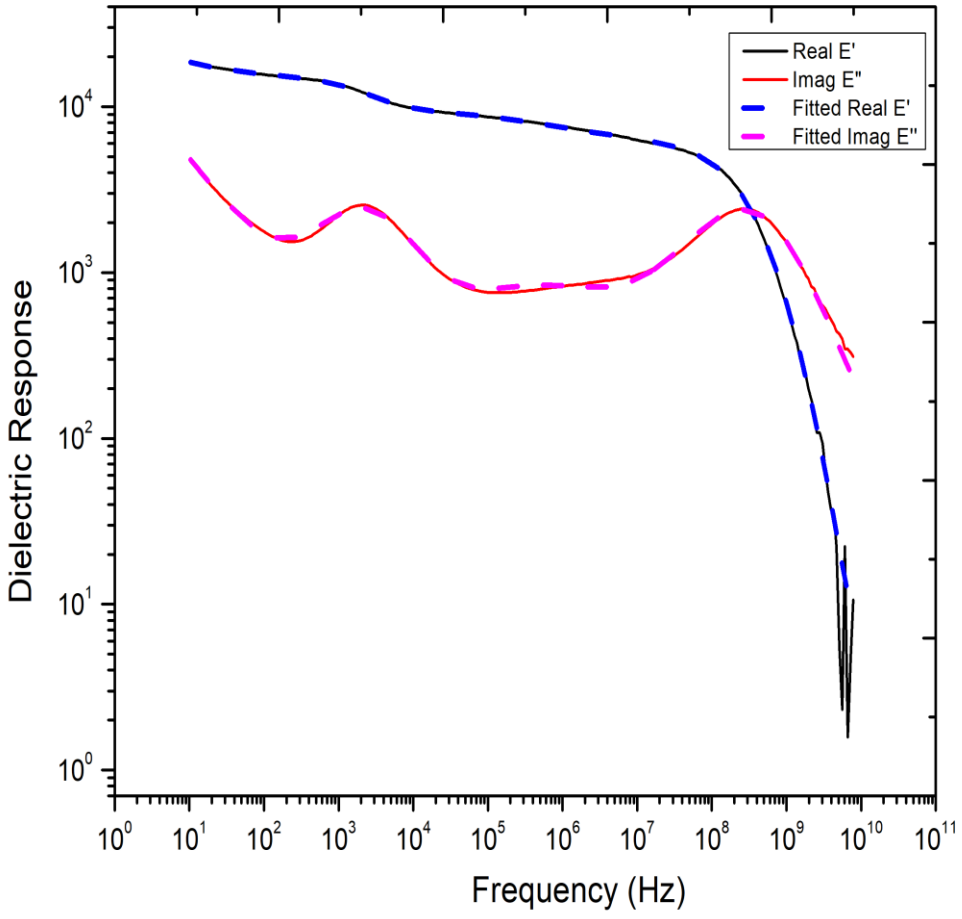

Fig. 21: Experimental and fitted dielectric permittivity ε'and dielectric loss ε″spectra of $Sr_{0.7}Nd_{0.2}TiO_3$ at 320 K.

From the fitting, two relaxation times were obtained for $Sr_{0.7}Nd_{0.2}TiO_3$. These relaxation times were marked as τ_1 and τ_2. The presence of two relaxation times shows that the dielectric response is not controlled by only one relaxation process. Since $SrTiO_3$-based ceramics can

have different contributions from defects, local polarization, charge movement and possibly grain or grain-boundary regions, the two relaxation times may be related to different polarization processes inside the sample. However, from the dielectric relaxation data alone, it is difficult to assign each relaxation time to one exact physical origin. Similar multiple relaxation processes have also been reported in $SrTiO_3$-based ceramics *[17]*.

The relaxation time is also connected with the frequency position of the dielectric relaxation response. When the relaxation feature shifts with temperature, the relaxation time also changes. In many dielectric materials, this behaviour can follow an Arrhenius-type relation. However, in $SrTiO_3$-based systems, the relaxation behaviour may not always follow one simple straight line because different defect-related or polarization processes can contribute to the response [17]. Unusual relaxation behaviour has also been reported in doped $SrTiO_3$ systems *[19]*.

In the present work, the extracted τ_1 and τ_2 values were plotted against 1000/T to check how both relaxation processes changed with temperature. Since τ_1 and τ_2 show different changes with temperature, they are discussed separately in the next section.

4.4.3 Temperature Dependence of Relaxation Times τ_1 and τ_2

After the relaxation times were taken from the fitting, τ_1 and τ_2 were plotted with 1000/T. This was done mainly to see how each relaxation process changes when the temperature changes. The plots are shown in Figure 22 and Figure 23. Here, log τ is used on the y-axis, so the relaxation time is shown in logarithmic form.

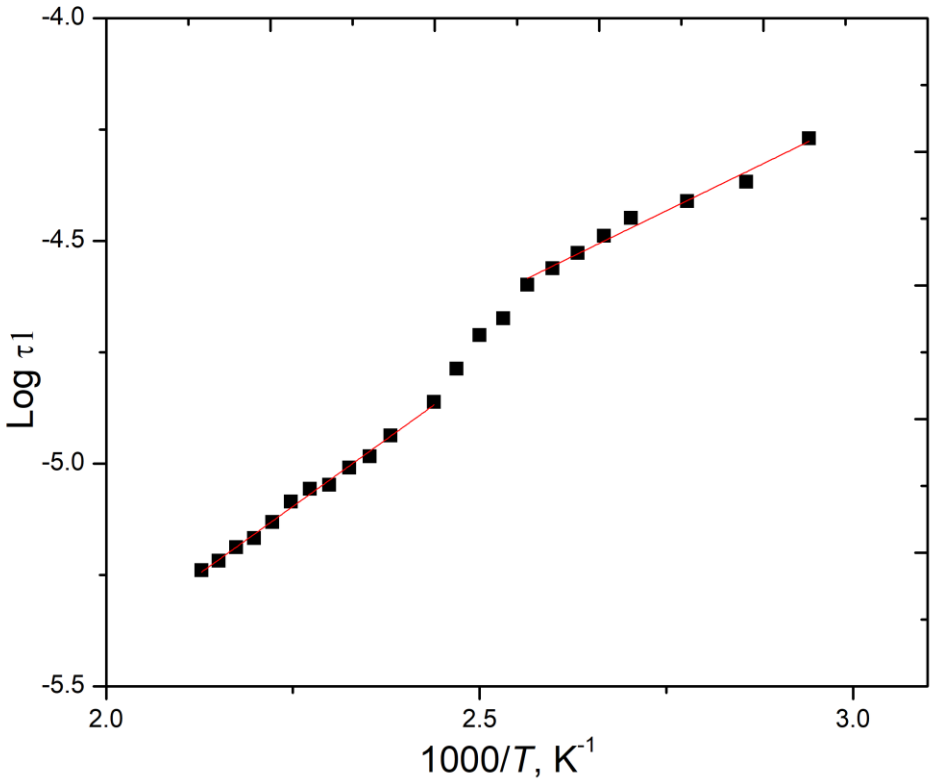

Fig. 22: Temperature dependence of log τ_1 for $Sr_{0.7}Nd_{0.2}TiO_3$.

Figure 22 shows the log τ_1 plot of $Sr_{0.7}Nd_{0.2}TiO_3$. In this graph, log τ_1 generally increases as 1000/T increases, which means that the relaxation time becomes larger when the temperature is reduced. This shows that the τ_1 relaxation process becomes slower during cooling. However, the plot does not follow one single linear trend over the full selected range. Two linear regions can be observed, with a change in slope around 400 K. This suggests that τ_1 may also be affected by a transition-like change or by a change in the dominant relaxation contribution.

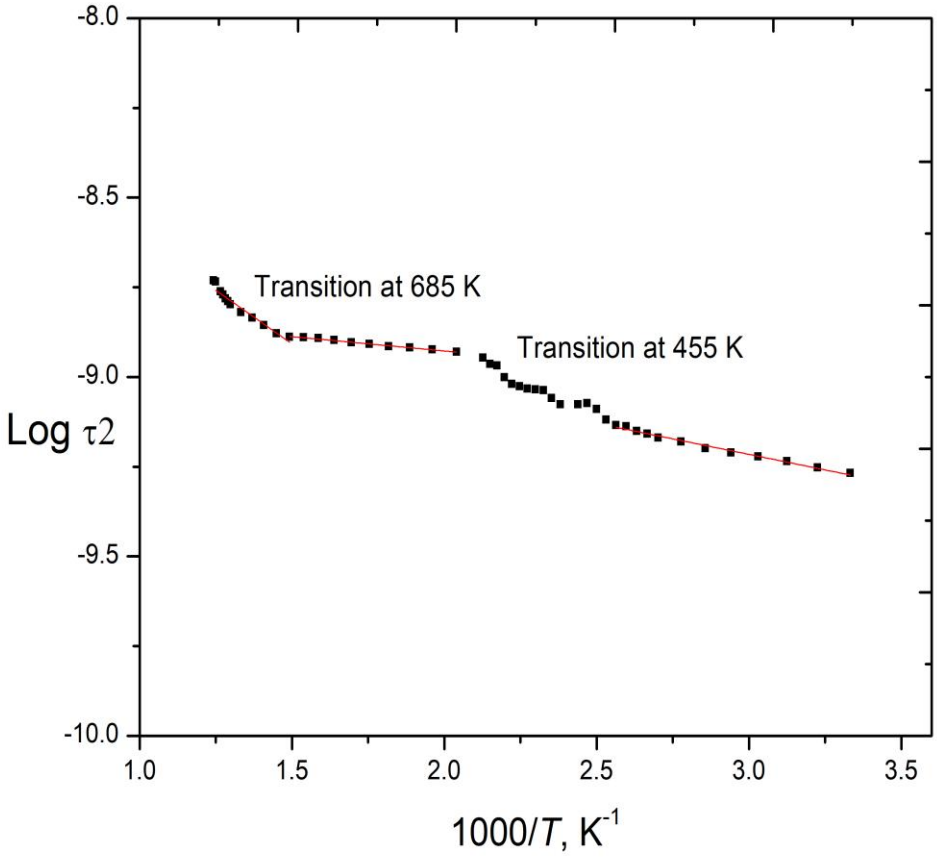

Fig. 23: Temperature dependence of log τ_2 for $Sr_{0.7}Nd_{0.2}TiO_3$. Transition-like changes are observed around 685 K and 455 K.

Figure 23 shows the log τ_2 plot for $Sr_{0.7}Nd_{0.2}TiO_3$. The τ_2 values do not follow one single straight line over the complete temperature range. Instead, the plot shows changes in slope in different regions. Two clear changes are observed around 685 K and 455 K. Because of this, τ_2 was not treated with one single fit, but was separated into three linear regions.

These different regions show that the τ_2 relaxation process changes with temperature. The slope changes noticeably across the different temperature ranges. Above 685 K, between 685 K and 455 K, and below 455 K, the relaxation behaviour follows different trends. This suggests that the same relaxation process is not dominant throughout the full temperature range. The changes

may be connected with defect-related polarization, localized charge movement, or lattice-related changes in the material. Similar non-simple relaxation behaviour has also been reported in doped $SrTiO_3$ systems *[17] [19].*

Overall, both τ_1 and τ_2 show changes in slope with temperature. This supports the idea that the dielectric relaxation behaviour of $Sr_{0.7}Nd_{0.2}TiO_3$ is influenced by more than one contribution. The observed changes may also be related to the structural transitions reported for this compound, especially because changes in the crystal structure can affect polarization and relaxation processes.

4.4.4 Activation Energy from Dielectric Relaxation

The activation energy from dielectric relaxation was calculated from the linear parts of the log τ versus 1000/T plots. This method is commonly used for relaxation analysis because the change of relaxation time with temperature can be connected with an Arrhenius-type relation *[17] [18].*Since the τ_1 and τ_2 plots both change slope, the fitting was done separately for each selected part. The final activation energy values are listed in Table 3.

Activation Energy from Dielectric Relaxation		
Relaxation process	**Temperature region**	**Activation energy, Ea (eV)**
τ_1	~470–410 K	0.24
τ_1	~390–340 K	0.16
τ_2	Above 685 K	0.12
τ_2	Between 685 K and 455 K	0.02
τ_2	Below 455 K	0.03

Table 3: Activation energy values obtained from the dielectric relaxation time analysis of $Sr_{0.7}Nd_{0.2}TiO_3$.

For τ_1, two regions were used from Figure 22. The fitted slope gives 0.24 eV in the 470–410 K range. At lower temperature, from 390–340 K, the value is reduced to 0.16 eV. This follows the slope change seen in the plot, so the τ_1 relaxation does not show the same temperature dependence throughout the selected range.

For τ_2, Figure 23 was divided into three fitted parts. The activation energy is 0.12 eV above 685 K. In the region between 685 K and 455 K, it drops to only 0.02 eV, which shows that τ_2 changes very little with temperature there. Below 455 K, the value rises slightly to 0.03 eV. This matches the transition-like changes already seen in the τ_2 plot.

The τ_2 activation energy values are lower than the τ_1 values, especially in the middle and lower temperature regions. This shows that the τ_2 relaxation process needs less energy in the selected regions. However, τ_2 does not follow one simple Arrhenius line, so these values should not be taken as one overall activation energy for the full τ_2 process. They are mainly useful for comparing the three fitted regions separately.

The difference between τ_1 and τ_2 shows that both relaxation times are not coming from the same response. The lower activation energy values for τ_2 may be connected with local charge movement, defect-related polarization, or changes in local polar regions. In $SrTiO_3$-based ceramics, dielectric relaxation can be affected by defects, oxygen vacancies, polar nanoregions and hopping-type processes *[17].* Rare-earth substituted $SrTiO_3$ ceramics can also show defect-related dielectric relaxation behaviour *[18].*

From this analysis, it can be seen that $Sr_{0.7}Nd_{0.2}TiO_3$ has more than one dielectric relaxation contribution. Both τ_1 and τ_2 show changes in slope, although the changes are more clearly separated in the τ_2 plot. Because of this, the dielectric relaxation behaviour of this sample cannot be explained by one single relaxation process.

Conclusions

After measuring the impedance spectra and conductivities across various temperature for the selected samples, the below are the conclusions:

- Most of the doped $SrTiO_3$ samples showed lower impedance and improved conductivity compared to the undoped $SrTiO_3$ sample. Among all the investigated samples, $Sr_{0.7}Nd_{0.2}TiO_3$ showed the strongest conductivity behaviour in the bulk ionic, total ionic and electronic conductivity graphs.
- Bulk ionic conductivity improved for several doped samples such as $Sr_{0.7}Nd_{0.2}TiO_3$, $Sr_{0.75}La_{0.25}TiO_3$ and $Sr_{0.65}La_{0.35}TiO_3$. These samples also gave lower bulk ionic activation energy values than the undoped STO sample. This indicates that ionic movement inside the material became easier after doping.
- In the total ionic conductivity graph, the conductivity behaviour was not same for all doped samples. $Sr_{0.85}Gd_{0.1}TiO_3$ showed better conductivity than $Sr_{0.7}Gd_{0.2}TiO_3$, while some La-doped samples such as $Sr_{0.85}La_{0.1}TiO_3$ and $Sr_{0.55}La_{0.3}TiO_3$ remained close to the undoped STO sample. This shows that grain boundary contribution still affected the total ionic transport behaviour.
- Electronic conductivity increased for many doped samples, especially for $Sr_{0.7}Nd_{0.2}TiO_3$. In the activation energy results, $Sr_{0.85}Gd_{0.1}TiO_3$ gave the highest electronic activation energy value, while smaller values were obtained for $Sr_{0.55}La_{0.3}TiO_3$ and $Sr_{0.7}Nd_{0.2}TiO_3$.
- Dielectric relaxation analysis of $Sr_{0.7}Nd_{0.2}TiO_3$ showed that both τ_1 and τ_2 do not follow one single trend over the full selected temperature range. For τ_1, two activation energy values were obtained, 0.24 eV and 0.16 eV. For τ_2, three regions were observed, with activation energy values of 0.12 eV, 0.02 eV and 0.03 eV. These results show that the dielectric response of this sample is not controlled by one single relaxation process.

References

1. Yuanyuan Wang, Shenghao Wang, Xueqing Yu, Lei Cao, Minmin Mao, Hadi Barzegar Bafrooei, Zhilun Lu, Kaixin Song, and Dawei Wang, Dramatic impact of raw chemicals on the electrical properties of $SrTiO_3$ ceramics, *Ceramics International* 50, 51841–51847 (2024).
2. Jinzhu Zhao. Etude th´eorique d'oxydes nano-structur´es multifonctionnels. Other. Univer sit´e Sciences et Technologies- Bordeaux I, 2013. French. PhD Thesis
3. Syed Zain Mehmood, Gul Rahman, M.S. Al-Buriahia, Nissren Tamam, and Imed Boukhris, Role of Sr and O vacancies in Gd-doped $SrTiO_3$: Insight from first-principles calculations, *Journal of Magnetism and Magnetic Materials* 628, 173109 (2025).
4. Xue Li, Hailei Zhao, Xiong Zhou, Nansheng Xu, Zhixiang Xie, and Ning Chen, Electrical conductivity and structural stability of La-doped $SrTiO_3$ with A-site deficiency as anode materials for solid oxide fuel cells, *International Journal of Hydrogen Energy* 35, 7913–7918 (2010).
5. Al Jumlata Ahmed, Sheikh Md. Kazi Nazrul Islam, Ridwone Hossain, Jeonghun Kim, Minjun Kim, Motasim Billah, Md. Shahriar A. Hossain, Yusuke Yamauchi, and Xiaolin Wang, Enhancement of thermoelectric properties of La-doped $SrTiO_3$ bulk by introducing nanoscale porosity, *Royal Society Open Science* 6, 190870 (2019).
6. Xue Li, Hailei Zhao, Dawei Luo, and Kevin Huang, Electrical conductivity and stability of A-site deficient (La, Sc) co-doped $SrTiO_3$ mixed ionic–electronic conductor, *Materials Letters* 65, 2646–2649 (2011).
7. Kai Guo, Fan Yang, Tianyao Weng, Jianguo Chen, Jiye Zhang, Jun Luo, Han Li, Guanghui Rao, and Jingtai Zhao, The electrical and thermal transport properties of La-doped $SrTiO_3$ with Sc_2O_3 composite, Materials 15(21), 7854 (2022).
8. Jia-Hong Lin, Chii-Shyang Hwang, and Fong-Ren Sie, Preparation and thermoelectric properties of Nd and Dy co-doped $SrTiO_3$ bulk materials, *Materials Research Bulletin* 122, 110650 (2020)
9. D. Popović, N. Romčević, S. Spasović, J. Dojčilović, A. Golubović, and S. Nikolić, Dielectric, spectral and Raman scattering studies of Nd-doped $SrTiO_3$ single crystal, Journal of Alloys and Compounds 425, 50–53 (2006).
10. A. Murashkina, E. Yu. Pikalova, and D. A. Medvedev, Gd-doped $SrTi_{0.5}Fe_{0.5}O_3$–δ mixed ionic–electronic conductors: Structural, thermal and electrical properties, *Ionics*, 23, 2351–2357 (2017)
11. Weidong Luo, Wenhui Duan, Steven G. Louie, and Marvin L. Cohen, Structural and electronic properties of n-doped and p-doped $SrTiO_3$, Physical Review B 70, 214109 (2004).
12. Miri Choi, Agham B. Posadas, Cesar A. Rodriguez, Andrew O'Hara, Heidi Seinige, Andrew J. Kellock, Martin M. Frank, Maxim Tsoi, Stefan Zollner, Vijay Narayanan, and Alexander A. Demkov, Structural, optical, and electrical properties of strained La-doped $SrTiO_3$ films, *Journal of Applied Physics* 116, 043705 (2014).
13. R. Li, C. Zhang, J. Liu, J. Zhou, and L. Xu, *A review on the electrical properties of doped $SrTiO_3$ as anode materials for solid oxide fuel cells*, Materials Research Express 6, 102006 (2019)

14. A. Pimenov, J. Ullrich, P. Lunkenheimer, A. Loidl, and C. H. Rüscher, Ionic conductivity and relaxations in ZrO_2–Y_2O_3 solid solutions, *Solid State Ionics* 109, 111–118 (1998).
15. I. Kosacki, H. U. Anderson, Y. Mizutani, and K. Ukai, Nonstoichiometry and electrical transport in Sc-doped zirconia, *Solid State Ionics* 152–153, 431–438 (2002).
16. Algimantas Kezionis, Saulius Kazlauskas, Dalius Petrulionis, and Antanas Feliksas Orliukas, Broadband Method for the Determination of Small Sample's Electrical and Dielectric Properties at High Temperatures, IEEE Transactions on Microwave Theory and Techniques 62(10), 2456–2461 (2014).
17. Xiaofei Wang, Qiubo Hu, Guozhong Zang, Chao Zhang, and Liben Li, Dielectric relaxation properties of $SrTiO_3$ ceramics modulated by stoichiometry, *Ceramics International* 44, 4740–4743 (2018).
18. Guangyao Li, Hanxing Liu, Zhijuan Wang, Hua Hao, Zhonghua Yao, Minghe Cao, and Zhiyong Yu, Dielectric properties and relaxation behavior of Sm substituted $SrTiO_3$ ceramics, *Journal of Materials Science: Materials in Electronics* 25, 4418–4424 (2014).
19. Zichen He, Minghe Cao, Eugene Furman, Michael T. Lanagan, Mengxue Yuan, Xiangyu Meng, Jinsong Wu, Hua Hao, Zhonghua Yao, Zhiyong Yu, and Hanxing Liu, Anomalous dielectric relaxation peak in Nb-doped $SrTiO_3$ single crystals, *Ceramics International* 48, 24725–24732 (2022).
20. Lazanas A.C., Prodromidis M.I. – *Electrochemical Impedance Spectroscopy—A Tutorial*. ACS Measurement Science Au 3(3), 162–193 (2023)
21. Schmidt R. – *Impedance Spectroscopy of Nanomaterials*. In CRC Concise Encyclopedia of Nanotechnology (eds. B.I. Kharisov, O.V. Kharissova, U. Ortiz-Mendez), pp. 364–382 (2016)
22. A. Kežionis, P. Butvilas, T. Šalkus, S. Kazlauskas, D. Petrulionis, T. Žukauskas, E. Kazakevičius, and A. F. Orliukas, *Four-electrode impedance spectrometer for investigation of solid ion conductors*, Review of Scientific Instruments 84, 013902 (2013).
23. Karmakar S. – *Impedance Spectroscopy for Electroceramics and Electrochemical System*. Advanced Energy Conversion Materials 6(1), 10–56 (2024)
24. Macdonald, J. R., & Barsoukov, E. (2005). *Impedance Spectroscopy: Theory, Experiment, and Applications* (2nd ed.). Wiley-Interscience.
25. Aljarrah M., Salman F. – *A Simple Analysis of Impedance Spectroscopy: Review*. Journal of The Institution of Engineers (India): Series D 102(1), 237–242 (2021)
26. Šarūnas Svirskas, Dzmitry Adamchuk, Robertas Grigalaitis, Džiugas Jablonskas, Jan Macutkevic, Giovanna Canu, Maria Teresa Buscaglia, Vincenzo Buscaglia, Lavinia Curecheriu, Liliana Mitoseriu, and Jūras Banys, Dipolar glass state in $BaCe_{0.3}Ti_{0.7}O_3$ perovskite solid solutions, *Journal of Alloys and Compounds* 854, 157555 (2021).
27. Huang J., Li Z., Liaw B.Y., Zhang J. – *Graphical analysis of electrochemical impedance spectroscopy data in Bode and Nyquist representations*. Journal of Power Sources 309, 82–98 (2016)
28. S.T. Bakenhaster and H.D. Dewald, *Electrochemical impedance spectroscopy and battery systems: Past work, current research, and future opportunities*, *Journal of Applied Electrochemistry* 55(2), 243–267 (2025)

Santrauka

Neenu Kelamangalath Sajeevan
Stroncio titanato, kuriame Sr dalinai pakeičiamas La, Gd arba Nd, elektrinių savybių tyrimas

Stroncio titanatas yra elektroninis ir joninis laidininkas. Šiame darbe stroncio titanatas, kuriame stroncis yra dalinai pakeičiamas lantanu, gadoliniu arba neodimiu, buvo ištirtas impedanso spektroskopijos metodais. Šio darbo tikslas buvo ištirti Sr^{2+} jonų pakeitimų Gd^{3+}, La^{3+} ir Nd^{3+} įtaką gautų naujų junginių keramikų elektrinėms savybėms. Matavimai buvo atlikti dažnių diapazone nuo 10 Hz iki 2 MHz, bandinių temperatūrą keičiant nuo 300 iki 800 K. Impedanso spektruose buvo stebimos dvi relaksacinio tipo dispersijos sritys. Pasitelkus ekvivalentines grandines, iš gautų impedanso spektrų buvo atskirti elektroninis ir joninis šių keramikų laidumai. Parodyta, kad atlikus dalinius joninius pakeitimus galima padidinti elektroninį ir joninį keramikų laidumus, o jų aktyvacijos energijos sumažėja. Be to, junginiui su Nd^{3+} buvo išanalizuoti dielektriniai spektrai, kurie leido nustatyti du fazinius virsmus vykstančius šioje medžiagoje.

Summary

Neenu Kelamangalath Sajeevan

Investigation of electrical properties of strontium titanate, in which Sr is partially substituted by La, Gd or Nd

Strontium titanate is an electronic and ionic conductor. In this work, strontium titanate, in which strontium is partially replaced by lanthanum, gadolinium or neodymium, was studied by impedance spectroscopy methods. The aim of this work was to investigate the influence of Sr^{2+} ion substitutions by Gd^{3+}, La^{3+} and Nd^{3+} on the electrical properties of the resulting new compound ceramics. Measurements were performed in the frequency range from 10 Hz to 2 MHz, with the sample temperature varying from 300 K to 800 K. Two relaxation-type dispersion regions were observed in the impedance spectra. Using equivalent circuits, the electronic and ionic conductivities of these ceramics were separated from the obtained impedance spectra. It was shown that partial ionic substitutions can increase the electronic and ionic conductivities of ceramics, and their activation energies decrease. In addition, the dielectric spectra of the compound with Nd^{3+} were analyzed, which allowed us to identify two phase transformations occurring in this material.